NAVAL POSTGRADUATE SCHOOL

MONTEREY, CALIFORNIA

THESIS

EFFECT OF NONLINEARITIES ON ORBIT COVARIANCE PROPAGATION

by

Christopher W. McLeod

September 2013

Thesis Advisor:	Kyle T. Alfriend
Second Reader:	I. Michael Ross

THIS PAGE INTENTIONALLY LEFT BLANK

REPORT DOCUMENTATION PAGE			Form Approved OMB No. 0704-0188
Public reporting burden for this collection of information is estimated to average 1 hour per response, including the time for reviewing instruction, searching existing data sources, gathering and maintaining the data needed, and completing and reviewing the collection of information. Send comments regarding this burden estimate or any other aspect of this collection of information, including suggestions for reducing this burden, to Washington headquarters Services, Directorate for Information Operations and Reports, 1215 Jefferson Davis Highway, Suite 1204, Arlington, VA 22202-4302, and to the Office of Management and Budget, Paperwork Reduction Project (0704-0188) Washington DC 20503.			
1. AGENCY USE ONLY ***(Leave blank)***	**2. REPORT DATE** September 2013	**3. REPORT TYPE AND DATES COVERED** Master's Thesis	
4. TITLE AND SUBTITLE EFFECT OF NONLINEARITIES ON ORBIT COVARIANCE PROPAGATION		**5. FUNDING NUMBERS**	
6. AUTHOR(S) Christopher W. McLeod			
7. PERFORMING ORGANIZATION NAME(S) AND ADDRESS(ES) Naval Postgraduate School Monterey, CA 93943-5000		**8. PERFORMING ORGANIZATION REPORT NUMBER**	
9. SPONSORING /MONITORING AGENCY NAME(S) AND ADDRESS(ES) N/A		**10. SPONSORING/MONITORING AGENCY REPORT NUMBER**	
11. SUPPLEMENTARY NOTES The views expressed in this thesis are those of the author and do not reflect the official policy or position of the Department of Defense or the U.S. Government. IRB Protocol number ____N/A____.			
12a. DISTRIBUTION / AVAILABILITY STATEMENT Approved for public release; distribution is unlimited		**12b. DISTRIBUTION CODE**	

13. ABSTRACT (maximum 200 words)

This thesis will examine the effect of nonlinearities on the propagation of orbit uncertainties in order to gain insight into the accurateness of the estimation of covariance with time. Many real-world applications rely on a first-order approximation of nonlinear equations of motion for propagation of orbit uncertainty. The nonlinear effects that are ignored during the linearization process can greatly influence the accuracy of the solution. A comparative analysis of linear and nonlinear orbit uncertainty propagation is presented in order to attempt to determine when linearized uncertainty becomes non-Gaussian. An examination of performance metrics is then accomplished to compare linearly propagated uncertainty to uncertainty propagated using a second-order approximation. An attempt is then made to develop a performance metric that determines when propagated uncertainty is no longer Gaussian. The results show it is difficult to determine a clear method of defining when the linear approximated uncertainty is no longer Gaussian, but there are metrics that can be implemented given a user-defined threshold of performance.

14. SUBJECT TERMS Space Situational Awareness, Orbital Mechanics, Non-Linear Covariance Propagation			**15. NUMBER OF PAGES** 81
			16. PRICE CODE
17. SECURITY CLASSIFICATION OF REPORT Unclassified	**18. SECURITY CLASSIFICATION OF THIS PAGE** Unclassified	**19. SECURITY CLASSIFICATION OF ABSTRACT** Unclassified	**20. LIMITATION OF ABSTRACT** UU

NSN 7540-01-280-5500

Standard Form 298 (Rev. 2-89)
Prescribed by ANSI Std. 239-18

THIS PAGE INTENTIONALLY LEFT BLANK

Approved for public release; distribution is unlimited

EFFECT OF NONLINEARITIES ON ORBIT COVARIANCE PROPAGATION

Christopher W. McLeod
Captain, United States Air Force
B.S., University of Colorado, 2006

Submitted in partial fulfillment of the
requirements for the degree of

MASTER OF SCIENCE IN SPACE SYSTEMS OPERATIONS

from the

NAVAL POSTGRADUATE SCHOOL
September 2013

Author: Christopher W. McLeod

Approved by: Dr. Kyle T. Alfriend
Thesis Advisor

Dr. I. Michael Ross
Second Reader

Dr. Rudolf Panholzer
Chair, Space Systems Academic Group

THIS PAGE INTENTIONALLY LEFT BLANK

ABSTRACT

This thesis will examine the effect of nonlinearities on the propagation of orbit uncertainties in order to gain insight into the accurateness of the estimation of covariance with time. Many real-world applications rely on a first-order approximation of nonlinear equations of motion for propagation of orbit uncertainty. The nonlinear effects that are ignored during the linearization process can greatly influence the accuracy of the solution. A comparative analysis of linear and nonlinear orbit uncertainty propagation is presented in order to attempt to determine when linearized uncertainty becomes non-Gaussian. An examination of performance metrics is then accomplished to compare linearly propagated uncertainty to uncertainty propagated using a second-order approximation. An attempt is then made to develop a performance metric that determines when propagated uncertainty is no longer Gaussian. The results show it is difficult to determine a clear method of defining when the linear approximated uncertainty is no longer Gaussian, but there are metrics that can be implemented given a user-defined threshold of performance.

THIS PAGE INTENTIONALLY LEFT BLANK

TABLE OF CONTENTS

LIST OF FIGURES

THIS PAGE INTENTIONALLY LEFT BLANK

LIST OF TABLES

THIS PAGE INTENTIONALLY LEFT BLANK

ACKNOWLEDGMENTS

I would like to extend my whole-hearted thanks to Dr. Terry Alfriend for his guidance, wisdom, and most importantly, his time spent helping me to understand some of the more challenging aspects of this topic. Your ability to take a complicated subject and transform it to something easily understood is remarkable. Dr. Mike Ross and everyone at the Naval Postgraduate School Space Systems Academic Group made getting here a fantastic experience. A special thanks to Dr. Josh Horwood and Dr. Kohei Fujimoto, whose insight helped me to get to some of the key points of the analysis. It was much appreciated. Finally, thanks most of all to my wife, Ashley, for her endless support. I love you.

THIS PAGE INTENTIONALLY LEFT BLANK

I. INTRODUCTION

This thesis will examine the effect of nonlinearities on the propagation of orbit uncertainties in order to gain insight into the accurateness of covariance estimation with time. Accurate covariance can be a valuable tool in space situational awareness. Covariance information can be used in the correlation of uncorrelated tracks (UCTs) [1]–[3], computing probability of collision [4] and sensor tasking [5].

Air Force Space Command (AFSPC) currently tracks over 22,000 orbiting objects via the Air Force Space Surveillance Network (SSN). When the SSN detects an object that does not correlate to an object in the Space Object Catalog, it is considered a UCT. Dr. Alfriend proves in [1] that the use of covariance for uncorrelated track association is the optimal measure as long as the uncertainties remain Gaussian. Provided the covariance is accurate, it can then be used to associate the UCT in a more statistically valid and automated manner than the current labor-intensive process [2]. In addition to UCT association, covariance is also useful in calculating the probability of collision between orbiting objects.

The increased reliance on space systems in recent history has led to increasing probability of collisions of on-orbit assets. A less accurate method of the collision avoidance calculation involves predicting conjunctions that fall within boxes centered on the two orbiting objects in question. The disadvantage of this is that it does not take into consideration the accuracy of the predicted boxes. Prior to launch of the International Space Station, NASA began using covariance for the probability of collision calculations. Other Department of Defense and national agencies have begun to use the same approach for predicting conjunctions and the ensuing probability of collision of on-orbit assets. Much like UCT association, an accurate covariance is a valuable tool in determining with greater precision the probability of collision between two objects that will pass close to each other [4]. In terms of determining whether spacecraft collision avoidance maneuvers are necessary, the accuracy of the probability of collision calculation can then be a key factor with respect to propellant conservation and on-orbit safety.

Most applications involving uncertainty propagation involve a linear approximation of a mathematical model of the nonlinear equations of motion. The linearization of the equations of motion for uncertainty propagation simplifies things a great deal; however the nonlinear effects that are ignored during this linearization process can greatly influence the accurateness of the solution. With this in mind, this thesis primarily attempts to answer two main questions. First, can examining the performance of nonlinear uncertainty propagation provide any insight into when the linear approximation fails? Second, which errors in the initial orbit uncertainty cause the propagated covariance to be non-Gaussian and how large do these errors have to be?

Through comparative analysis of linear and nonlinear orbit uncertainty propagation techniques, we can attempt to determine when the effects of the nonlinearities cause the inaccuracy of the covariance to be large enough to render it no longer useful. In order to gain insight into when the linear approximation fails, this thesis will consider the classical orbital elements and two-body motion with a comparison of a first-order approximation to a second-order approximation.

Chapter II is a background chapter. It gives a brief review of the Clohessy-Wiltshire equations, the definition of the orbit state that will be used and then an overview of the higher order approximation that will be used in the comparative analysis. Chapter III presents the results of the comparative analysis and Chapter IV addresses the topic of determining appropriate metrics to assess the performance of a first-order approximation.

II. BACKGROUND

A. FORMULATION OF THE PROBLEM

1. Overview

Expressions that describe the dynamics of orbital motion are based on a set of nonlinear differential equations. However, in many real-world applications, the propagation of uncertainty is accomplished using a first-order approximation. Given initial Gaussian uncertainty, the propagated uncertainty remains Gaussian as long as the system remains linear. The system however is nonlinear, and eventually the neglected nonlinearities influence the accuracy of the propagated covariance.

The dynamics of uncertainty propagation are often described using a first-order approximation. More complex models exist; however selecting the appropriate model is a balance between simplicity and accuracy. With increased accuracy, comes higher cost in terms of computation time, computing resources and overall problem complexity. Insight into when a particular mathematical model is no longer valid or when it no longer meets requirements is very useful. Determining this threshold will be the primary focus of this thesis. Previous work by Fujimoto et al. [6], and Park and Scheeres [7], has shown significant increases in model accuracy can be obtained by using a second-order approximation. Much of the comparative analysis presented in this thesis relies on a comparison of second-order to first-order approximation for covariance propagation.

The background information presented in the remainder of this chapter consists of a brief review of the Clohessy-Wiltshire (CW) equations, the definition of the orbit state, and then presents an overview of the higher order approximation that will be used for comparative analysis.

2. Linearized Model

A linearized mathematical model is useful for describing the motion of an orbiting vehicle relative to a reference orbit. The well-known Clohessy-Wiltshire equations provide a linearized model that approximates relative orbital motion. The CW equations

are the linearization of the equations of motion about a circular orbit and spherical Earth. Although there are more complicated linearized models that consider non-circular orbits and perturbations [8], the CW equations can be useful for demonstrating the types of relative motion obtained by closely orbiting objects. The derivations of the CW equations can be found in found in [9]. For purposes of this thesis, the CW equations are merely stated. The CW equations are:

$$\begin{aligned} \ddot{x} - 2n\dot{y} - 3n^2 x &= 0 \\ \ddot{y} + 2n\dot{x} &= 0 \\ \ddot{z} + n^2 z &= 0 \end{aligned} \tag{1.1}$$

where n is the mean motion defined by:

$$n = \sqrt{\frac{\mu}{r^3}} \tag{1.2}$$

The solutions for the CW equations are given by the following:

$$\begin{aligned} x &= \left(4 - 3\cos\left(nt\right)\right)x_0 + \left(\frac{\dot{x}_0}{n}\right)\sin\left(nt\right) + \left(\frac{2\dot{y}_0}{n}\right)\left(1 - \cos\left(nt\right)\right) \\ y &= 6\left(\sin\left(nt\right) - nt\right)x_0 + 2\left(\frac{\dot{x}_0}{n}\right)\cos\left(nt\right) + y_0 + \left(\frac{\dot{y}_0}{n}\right)\left(4\sin\left(nt\right) - 3nt\right) \\ z &= z_0\cos\left(nt\right) + \left(\frac{\dot{z}_0}{n}\right)\sin\left(nt\right) \end{aligned} \tag{1.3}$$

The CW frame is illustrated in Figure 1. The x-axis or radial component lies along the object's radius vector. The y-axis or in-track component lies in the orbit plane perpendicular to the x-axis. The z-axis or cross-track component is perpendicular to the orbit plane. The origin of the CW frame moves with the reference object and is a rotating frame. The angular velocity of the rotating frame is equal to the orbital angular velocity. This coordinate system is also referred to as the radial, in-track, cross-track or RIC frame and is very useful when discussing differences between two orbits.

The motion of an anecdotal low earth orbit object under the CW model is illustrated in Figure 2. One can see that the motion in the radial and cross-track directions are periodic and do not grow in magnitude under the linear assumption. The in-track motion does change significantly with time. It is the growth in the in-track direction that has higher order effects on the linear model and causes the uncertainty to no longer be Gaussian. The goal is to determine when this happens as a function of time and initial uncertainties. The secular term from Equation (1.3) is given by:

$$Secular\ Motion = \left(-6nx_0 - 3\dot{y}_0\right)t \tag{1.4}$$

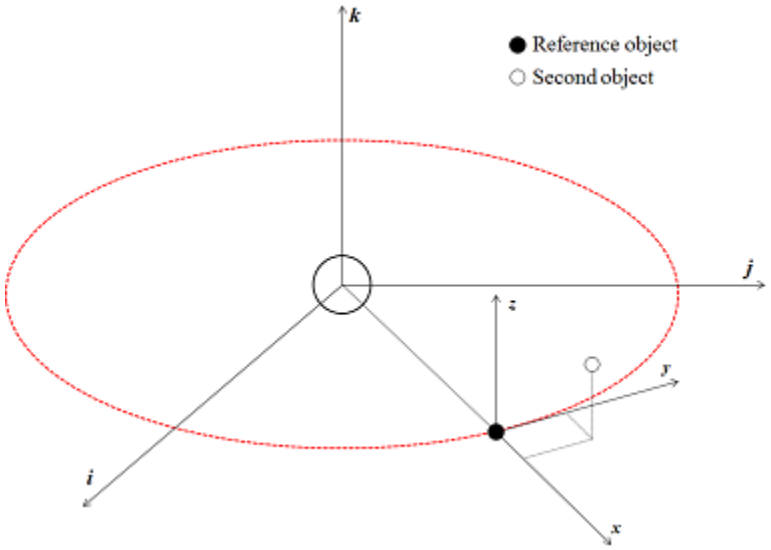

Figure 1. Clohessy-Wiltshire Frame

In terms of differential motion in the orbital elements in the CW model, inclination, right ascension of the ascending node and eccentricity all cause periodic variations. The in-track secular motion is caused by differentials in the mean anomaly and semi-major axis. In an attempt to isolate the non-Gaussian behavior caused by the secular motion in the in-track direction, the two-dimensional state of mean anomaly and semi-major axis will be used. This 2D state should capture the essential elements of the nonlinear behavior that causes the non-Gaussian behavior of the uncertainty.

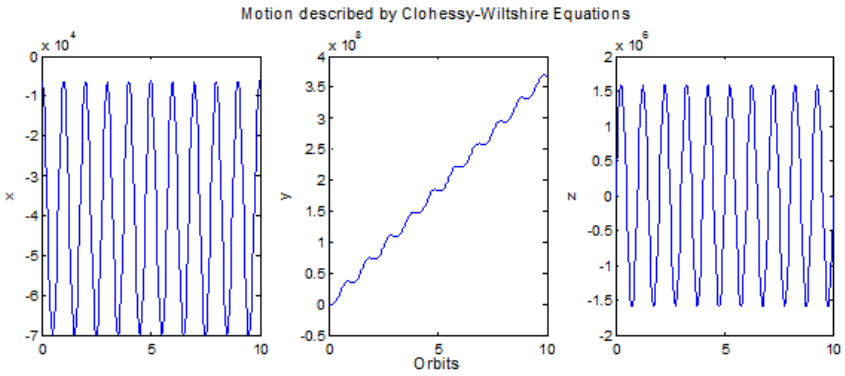

Figure 2. Motion Described by CW Equations

3. Definition of the State

In an attempt to isolate the non-Gaussian behavior caused by the secular motion in the in-track direction, the state considered for this thesis will consist of the semi-major axis and mean anomaly. The dynamics of an n dimensional system can be expressed as:

$$\begin{aligned} \dot{\mathbf{x}} &= f\left(t, \mathbf{x}\right) \\ \mathbf{x}^T &= \left(x_1, x_2, ..., x_n\right) \end{aligned} \tag{1.5}$$

where the solution to Equation (1.5) is given by:

$$\mathbf{x}\left(t\right) = \phi\left(t, \mathbf{x}_0, t_0\right) \tag{1.6}$$

and $\mathbf{x}_0$ is the initial state at time t_0. Given the reference solution $\overline{\mathbf{x}}\left(t, t_0\right)$, the state deviation vector can be represented by:

$$\delta\mathbf{x} = \mathbf{x}\left(t\right) - \overline{\mathbf{x}}\left(t\right) \tag{1.7}$$

It follows then that:

$$\delta\dot{\mathbf{x}} = f\left(t, \mathbf{x}\right) - f\left(t, \overline{\mathbf{x}}\right) \tag{1.8}$$

The analysis presented will consist of the two dimensional state consisting of the change in semi-major axis and mean anomaly. The "truth" state consists of two-body

motion with no perturbations. The equations of motion for the two dimensional state are expressed in Equation (1.9):

$$\begin{aligned} a &= a_0 \\ \dot{a} &= 0 \\ M &= \sqrt{\frac{\mu}{a^3}}t + M_0 \\ \dot{M} &= \sqrt{\frac{\mu}{a^3}} = n \end{aligned} \tag{1.9}$$

The highest order approximation used for this analysis will be to second-order. Although a higher order approximation does provide a more accurate solution, the most significant performance gain over the linear approximations comes from the second-order approximation. To obtain the equations that approximate the motion, we will expand in a Taylor series about the reference orbit to second-order.

The state is given by:

$$\delta\mathbf{x} = \begin{bmatrix} \delta a^* \\ \delta M \end{bmatrix} \tag{1.10}$$

where the "*" notation indicates a normalized dimensionless term. The non-dimensional change in semi-major axis is given by:

$$\delta a^* = \frac{\delta a}{\bar{a}} \tag{1.11}$$

where the "bar" notation denotes the value on the reference orbit. The time scale used will be expressed in terms of number of orbits, τ. The time scale is given by:

$$\tau = \frac{\bar{n}t}{2\pi} \tag{1.12}$$

The expressions for the change in semi-major axis and mean anomaly (expanded to second-order) become:

$$\delta a^* = \delta a_0^*$$
$$\delta M = \left[-3\pi\delta a^* + \frac{15\pi}{4}\left(\delta a^*\right)^2 \right]\tau + \delta M_0 \tag{1.13}$$

Finally, using the first-order term from Equation (1.13), the linearized state transition matrix is:

$$\Phi(\tau) = \begin{pmatrix} 1 & 0 \\ -3\pi\tau & 1 \end{pmatrix} \tag{1.14}$$

4. Nonlinear Uncertainty Mapping

Equation (1.14) is the familiar linear state transition matrix determined by a first-order approximation. In order to capture the nonlinear behavior neglected in the linear approximation, Park and Scheeres [10] proposed a higher order method of approximating an orbit state and covariance by incorporating the higher order Taylor series terms. The higher order state solutions as a function of initial conditions are referred to as state transition tensors (STT).

From Park and Scheeres [10], the state deviation vector $\delta\mathbf{x}$, the mean deviation vector $\delta\mathbf{m}$, as well as the uncertainty $\mathbf{P}$, expanded to second-order are given by:

$$\delta\mathbf{x}_i = \phi_{i,k}\delta x_k^0 + \frac{1}{2}\left(\phi_{i,ab}\delta x_a^0 \delta x_b^0\right) \tag{1.15}$$
$$\delta\mathbf{m}_i = \frac{1}{2}\left(\phi_{i,ab}P_{ab}^0\right) \tag{1.16}$$
$$\mathbf{P}_{ij} = \phi_{i,a}\phi_{j,\alpha}P_{a\alpha}^0 - \delta m_i \delta m_j + \frac{1}{4}\phi_{i,ab}\phi_{j,\alpha\beta}\left(P_{ab}^0 P_{\alpha\beta}^0 + P_{a\alpha}^0 P_{b\beta}^0 + P_{a\beta}^0 P_{b\alpha}^0\right) \tag{1.17}$$

Where $\delta\mathbf{x}_0$ and $\mathbf{P}^0$ are the initial state and covariance, respectively. Einstein's summation notation is used here and the subscripts "*i*" and "*k*", respectively represent the *i*th and kth component. Given the state vector from Equation (1.10) and (1.13), the state transition tensors expressed non-dimensionally are:

$$\Phi_{i,k}(\tau)=\frac{\partial\delta\mathbf{x}}{\partial\delta\mathbf{x}}=\begin{pmatrix}1 & 0\\ -3\pi\tau & 1\end{pmatrix}$$
$$\Phi_{i,1b}(\tau)=\frac{\partial^2\delta\mathbf{x}}{\partial\delta\mathbf{x}\partial\delta a^*}=\begin{pmatrix}0 & 0\\ \frac{15}{2}\pi\tau & 0\end{pmatrix} \tag{1.18}$$
$$\Phi_{i,2b}(\tau)=\frac{\partial^2\delta\mathbf{x}}{\partial\delta\mathbf{x}\partial\delta M}=\begin{pmatrix}0 & 0\\ 0 & 0\end{pmatrix}$$

The first of Equation (1.18) represents the familiar linear state transition matrix. The second and third of Equation (1.18) are the STTs and represent the contributions from the second-order Taylor series expansion. One can see from the expressions for the second-order STTs in Equation (1.18), all the higher order terms are zero with the exception of the $\Phi_{2,11}$ term, which represents the second partial derivative of δM with respect to $\left(\delta a^*\right)^2$.

$$\Phi_{2,11}=\frac{\partial^2\delta M}{\partial\delta a^{*2}} \tag{1.19}$$

Due to many of the higher order terms in the STTs being equal to zero, the expressions for the state, mean, and particularly the covariance can be simplified a great deal. The expression for the state given in Equation (1.15) expanded from Einstein's summation notation is written as:

$$\delta\mathbf{x}_i=\begin{bmatrix}\phi_{1,1}\delta x_1^0+\phi_{1,2}\delta x_2^0+\frac{1}{2}\left(\phi_{1,11}\delta x_1^0\delta x_1^0+\phi_{1,12}\delta x_1^0\delta x_2^0+\phi_{1,21}\delta x_2^0\delta x_1^0+\phi_{1,22}\delta x_2^0\delta x_2^0\right)\\ \phi_{2,1}\delta x_1^0+\phi_{2,2}\delta x_2^0+\frac{1}{2}\left(\phi_{2,11}\delta x_1^0\delta x_1^0+\phi_{2,12}\delta x_1^0\delta x_2^0+\phi_{2,21}\delta x_2^0\delta x_1^0+\phi_{2,22}\delta x_2^0\delta x_2^0\right)\end{bmatrix} \tag{1.20}$$

Given initial $\delta\mathbf{x}_0$:

$$\delta\mathbf{x}_0=\begin{bmatrix}\delta a_0^*\\ \delta M_0\end{bmatrix} \tag{1.21}$$

when one simplifies Equation (1.20) and discards the terms that equal zero, the equation for the state deviation vector as a function of non-dimensional time τ is:

$$\delta \mathbf{x}_i(\tau) = \begin{bmatrix} \delta a_0^* \\ \left(-3\pi\delta a_0^* + \frac{15\pi}{4}\left(\delta a_0^*\right)^2\right)\tau + \delta M_0 \end{bmatrix} \tag{1.22}$$

Note that the second term of Equation (1.22) is simply the second-order Taylor series expansion of δM shown in Equation (1.13). In fact Equation (1.22) and Equation (1.13) are equivalent expressions.

The second-order mean deviation vector from Equation (1.16) is expressed as:

$$\delta \mathbf{m}_i = \begin{bmatrix} \frac{1}{2}\left(\phi_{1,11}P_{1,1}^0 + \phi_{1,12}P_{1,2}^0 + \phi_{1,21}P_{2,1}^0 + \phi_{1,22}P_{2,2}^0\right) \\ \frac{1}{2}\left(\phi_{2,11}P_{1,1}^0 + \phi_{2,12}P_{1,2}^0 + \phi_{2,21}P_{2,1}^0 + \phi_{2,22}P_{2,2}^0\right) \end{bmatrix} \tag{1.23}$$

however, once simplified by combining with Equation (1.18), the mean shown in Equation (1.23) reduces to:

$$\delta \mathbf{m}(\tau) = \begin{bmatrix} 0 \\ \frac{15\pi}{2} P_{1,1}^0 \tau \end{bmatrix} \tag{1.24}$$

The expansion from Einstein's notation of the second-order covariance is left for the Appendix. After combining the expression for the covariance in Equation (1.17) and the STTs from Equation (1.18), and simplifying terms equal to zero, the approximation for the second-order covariance can be expressed as:

$$\mathbf{P}_{ij} = \begin{bmatrix} \phi_{1,1}\phi_{1,1}P_{11}^0 & \phi_{1,1}\phi_{2,1}P_{11}^0 \\ \phi_{2,1}\phi_{1,1}P_{11}^0 & \phi_{2,1}\phi_{2,1}P_{11}^0 + \phi_{2,2}\phi_{2,2}P_{22}^0 - \delta m_2 \delta m_2 + \frac{1}{4}\left[\phi_{2,11}\phi_{2,11}\left(P_{11}^0 P_{11}^0 + P_{11}^0 P_{11}^0 + P_{11}^0 P_{11}^0\right)\right] \end{bmatrix} \tag{1.25}$$

or as a function of time τ,

$$\mathbf{P}(\tau)=\begin{bmatrix} P_{11}^{0} & -3\pi\tau P_{11}^{0} \\ -3\pi\tau P_{11}^{0} & \left(9P_{11}^{0}+\frac{225}{8}\left(P_{11}^{0}\right)^{2}\right)\pi^{2}\tau^{2}+P_{22}^{0} \end{bmatrix} \tag{1.26}$$

Using Equation (1.22) and (1.26) we can now propagate the state and covariance using a second-order approximation.

THIS PAGE INTENTIONALLY LEFT BLANK

III. COVARIANCE ANALYSIS

A. INTRODUCTION

This section examines covariance propagation through comparison of uncertainty ellipsoid propagation and Monte Carlo simulations. The cumulative probability distribution for first-order and second-order approximations compared to the theoretical distribution for a linear system is also presented. To begin, we will examine how uncertainty propagates under the first-order and second-order approximations.

B. ELLIPSE PROPAGATION

For the uncertainty ellipse propagation, a demonstration of how an initial Gaussian distribution propagates under unperturbed two-body equations of motion is presented. Only the two dimensional state consisting of δa^* and δM is considered.

For the error ellipsoid analysis presented in this section, 10^6 points on the initial 3σ uncertainty ellipse are propagated using the linear approximation given by the state transition matrix in Equation (1.14). The points are also propagated using the second-order approximation given in Equation (1.13). A Monte Carlo simulation is then performed by propagating 10^6 normally distributed points obtained from the initial uncertainty. The Monte Carlo points are propagated using the complete system dynamics:

$$\begin{aligned} \delta a^* &= \delta a_0^* \\ \delta M = M - \bar{M} &= \left(\sqrt{\frac{\mu}{(\bar{a} + \delta a)^3}} t + M_0 \right) - \left(\sqrt{\frac{\mu}{\bar{a}^3}} t + \bar{M}_0 \right) \end{aligned} \tag{2.1}$$

Note that Equation (2.1) is not expressed in dimensionless terms or in the timescale τ. The following shows the expressions for the state in non-dimensional terms. The non-dimensional semi-major axis is:

$$a^* = \frac{a}{\bar{a}} \tag{2.2}$$

where the "bar" over the variable represents a value on the reference orbit. The non-dimensional time is given by:

$$\tau = \frac{\bar{n}t}{2\pi} \tag{2.3}$$

Given that the semi-major axis is:

$$a = \bar{a} + \delta a \tag{2.4}$$

the normalized semi-major axis is

$$a^* = 1 + \delta a^* \tag{2.5}$$

The expression for mean anomaly is:

$$M = nt + M_0 \tag{2.6}$$

Substituting τ into Equation (2.6) for non-dimensional terms yields:

$$\begin{aligned} M &= 2\pi\left(\frac{n}{\bar{n}}\right)\tau + M_0 = 2\pi\sqrt{\frac{\bar{a}^3}{a^3}}\tau + M_0 \\ M &= 2\pi\left(a^*\right)^{-3/2}\tau + M_0 \end{aligned} \tag{2.7}$$

Note that:

$$\begin{aligned} \frac{da^*}{d\tau} &= 0 \\ \frac{dM}{d\tau} &= 2\pi\left(a^*\right)^{-3/2} \end{aligned} \tag{2.8}$$

Therefore, given that $\delta M = M - \bar{M}$ the exact solution for the change in mean anomaly is:

$$\delta M_{exact} = 2\pi\left[\left(a^*\right)^{-3/2} - 1\right]\tau + \delta M_0 \tag{2.9}$$

1. Ellipse Propagation Results

By propagating the 3σ uncertainty ellipsoid using first and second-order propagations and comparing to the exact propagation of the Monte Carlo points, we are able to examine the validity of the approximations at various propagation times. For this scenario, the uncertainty is given by:

$$\boldsymbol{P}_0 = \begin{pmatrix} \sigma_{\delta a^*}^2 & 0 \\ 0 & \sigma_{\delta M}^2 \end{pmatrix} \tag{2.10}$$

where the semi-major axis uncertainty is 21 km, the mean anomaly uncertainty is 0.01° and the reference semi-major axis is $\bar{a} = 7000\,km$. Given these parameters, the orbital period is 1.619 hours. The standard deviations are given by:

$$\begin{aligned} \sigma_{\delta a^*} &= \frac{\sigma_{\delta a}}{\bar{a}} = \frac{21\,km}{7000\,km} = 0.003 \\ \sigma_{\delta M} &= 0.01^\circ \end{aligned} \tag{2.11}$$

The initial distribution as well as the 3σ ellipse based on the initial uncertainty $\mathbf{P}_0$ are shown in the top left of Figure 3. The remaining plots are the 3σ ellipse propagated using first and second-order approximations, as well as the Monte Carlo points propagated using the complete system dynamics at 2, 5, and 10 orbits.

The green ellipse represents the 3σ ellipse propagated using a first-order approximation from Equation (1.14) and the blue dashed ellipse is the second-order approximation from Equation (1.13). The $\delta a^* - \delta M$ plane is rotated so the principal axes of the linearly propagated ellipse are aligned with the horizontal and vertical axis of the plot. Ideally, the propagated ellipse should continue to capture a large number of the Monte Carlo sample points. One can see that the accuracy of the linearly propagated ellipse capturing the sample points significantly degrades with time.

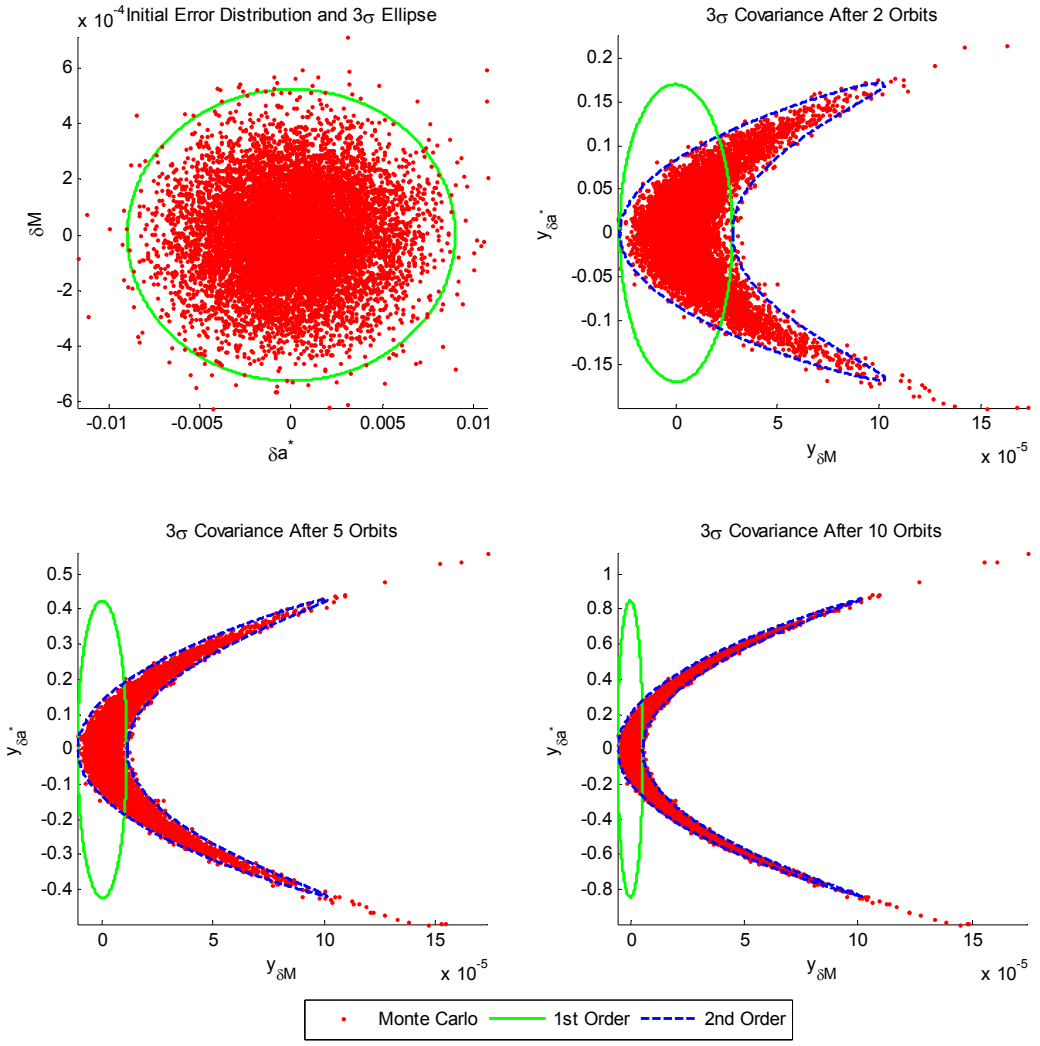

Figure 3. Initial Gaussian Distribution and Propagated Gaussian Distribution with Corresponding 3σ Ellipsoids

The theoretical distribution for a two-dimensional system is given by:

$$F(k) = 1 - e^{\frac{-k^2}{2}} \tag{2.12}$$

where k represents the number of standard deviations. For k=3, the theoretical probability distribution is 0.9889, i.e., the 3σ ellipse should capture 98.89% of the Monte Carlo sample points. As seen in Table 1, for the initial uncertainty given in (2.11), by 10 orbits the linear propagation has failed to represent a significant portion (nearly half) of

the system dynamics. The illustrations in Figure 3 show the second-order propagation does a much better job of characterizing the full system dynamics. The results of the probability distribution captured by the first-order 3σ ellipse are summarized in Table 1.

Theoretical	Initial	2 Orbits	5 Orbits	10 Orbits
0.9889	0.9992	0.8383	0.6512	0.5045

Table 1. Linear Probability Distribution through 10 Orbits

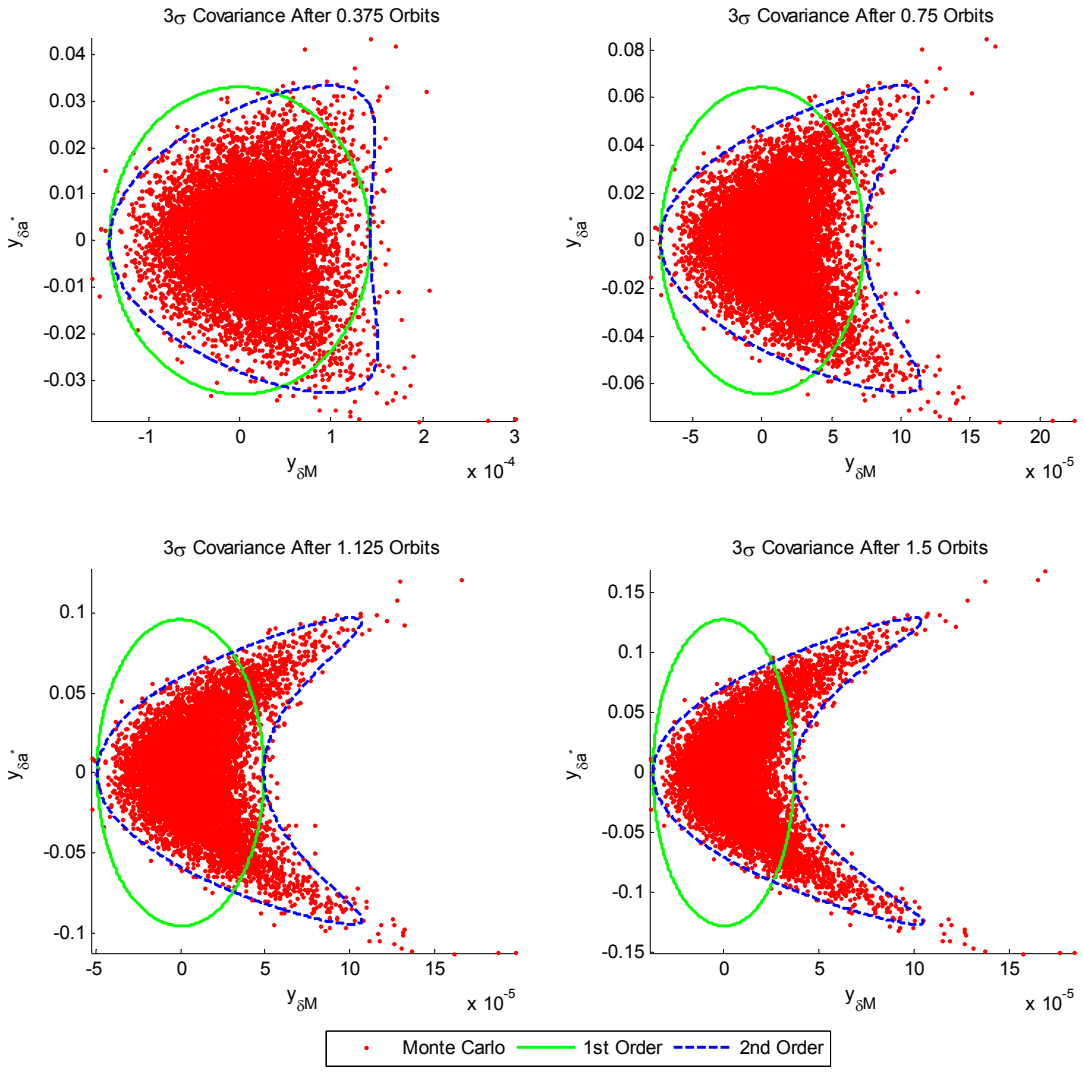

Figure 4. Propagated Gaussian Distributions with Corresponding 3σ Ellipsoids

Although the linear propagation does not fully represent the full system dynamics, for a short propagation time, the first-order approximation may be acceptable. One can see that at 2 orbits, or 3.24 hours, the first-order approximation still encompasses 83.8 % of the sample points.

Figure 4 illustrates the results of various propagation times out to 1.5 orbits. Again, the propagated covariance is rotated so the primary axes of the linear ellipse correspond to the axes of the plot. One can see via the distortion of the second-order ellipsoid and the Monte Carlo distribution, there are higher order effects even at 0.375 orbits, or just over 30 minutes of propagation time. Despite some loss from nonlinear effects, depending on the accuracy required, the linear approximation at shorter propagation times may be sufficient. Table 2 summarizes the numerical results for the probability distribution captured by the linear approximation.

Theoretical	**Initial**	**0.375 Orbits**	**0.75 Orbits**	**1.125 Orbits**	**1.5 Orbits**
0.9889	0.9992	0.9783	0.9498	0.9167	0.8825

Table 2. Linear Probability Distribution through 1.5 Orbits

2. Ellipse Rotation

The ellipse rotation consists of rotating the major and minor axis of the first-order ellipse to correspond to the primary axes of the plot. This allows a closer examination of the higher order effects. The second-order contribution to δM comes from the following term of Equation (1.22):

$$\frac{15\pi}{4}\left(\delta a_0^*\right)^2 \tau \tag{2.13}$$

Figure 5 shows the non-rotated covariance ellipsoids propagated to two orbits using the same standard deviations given in (2.11). The plot on right of Figure 5 is zoomed in to show the second-order ellipse curvature.

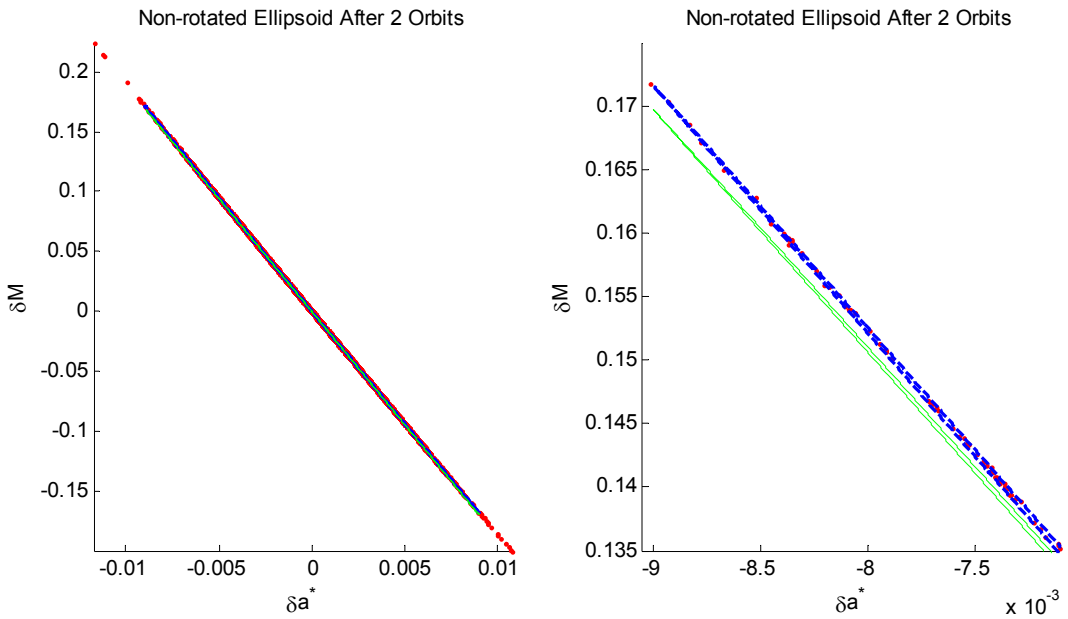

Figure 5. Non-Rotated Covariance Ellipsoids after Two Orbits

The higher order contribution to δM is small compared to the total value of δM but it is large compared to the ellipsoid minor axis. A property of linearly propagated covariance is that the area of the linear ellipsoid is constant with time. The covariance does not grow in the δa^* direction, so as it grows in the δM direction, the ellipse becomes thinner with time along the minor axis.

To examine the higher order effects it is necessary to determine a coordinate system where the first-order covariance is diagonal. This will rotate the axes of the linearly propagated covariance to the primary axes of the plot. To do so, we use the following:

$$\delta \mathbf{y} = \mathbf{R}\delta \mathbf{x} \tag{2.14}$$

where $\delta \mathbf{x}$ is the state given Equation (1.22) and $\delta \mathbf{y}$ is the rotated state:

$$\delta \mathbf{y} = \begin{bmatrix} y_{\delta M} \\ y_{\delta a^*} \end{bmatrix} \tag{2.15}$$

R is the clockwise rotation matrix:

$$\mathbf{R} = \begin{bmatrix} \cos\theta & \sin\theta \\ -\sin\theta & \cos\theta \end{bmatrix} \tag{2.16}$$

The covariance rotation is accomplished by:

$$\mathbf{P}_y = \mathbf{R}\mathbf{P}_x\mathbf{R}^T \tag{2.17}$$

where $\mathbf{P}_x$ is the linearly propagated covariance

$$\mathbf{P}_x = \begin{bmatrix} P_{x11} & P_{x12} \\ P_{x12} & P_{x22} \end{bmatrix} \tag{2.18}$$

and the rotated covariance $\mathbf{P}_y$ is given by:

$$\mathbf{P}_y = \begin{bmatrix} P_{y11} & P_{y12} \\ P_{y12} & P_{y22} \end{bmatrix} \tag{2.19}$$

which gives:

$$\begin{aligned} P_{y11} &= \frac{1}{2}\left(P_{x11} + P_{x22}\right) + \frac{1}{2}\left(P_{x11} - P_{x22}\right)\cos\left(2\theta\right) + P_{x12}\sin\left(2\theta\right) \\ P_{y22} &= \frac{1}{2}\left(P_{x11} + P_{x22}\right) - \frac{1}{2}\left(P_{x11} - P_{x22}\right)\cos\left(2\theta\right) - P_{x12}\sin\left(2\theta\right) \\ P_{y12} &= P_{x12}\cos\left(2\theta\right) - \frac{1}{2}\left(P_{x11} - P_{x22}\right)\sin\left(2\theta\right) \end{aligned} \tag{2.20}$$

To obtain the coordinate system where the covariance is diagonal, we set $P_{y12} = 0$ and solve for the rotation angle θ:

$$\theta = \frac{1}{2}\arctan\left(\frac{2P_{x12}}{P_{x11} - P_{x22}}\right) \tag{2.21}$$

or

$$\theta = \frac{1}{2}\arctan\left(\frac{2\left(\sigma_{\delta a^*}\sigma_{\delta M}\right)}{\left(\sigma_{\delta a^*}\right)^2 - \left(\sigma_{\delta M}\right)^2}\right) \tag{2.22}$$

The rotation angle obtained from Equation (2.22) is then used with the rotation matrix given by Equation (2.16).

C. PROBABILITY DISTRIBUTION

1. Overview

This section examines the cumulative probability distribution using the first and second-order approximation as well as the exact solution for covariance propagation. The results of the probability distribution are compared to the theoretical cumulative distribution function to assess the performance of the approximation. The Gaussian multivariate probability density function is:

$$f(\mathbf{x}) = \frac{1}{\left(2\pi\right)^{N/2}\left|\mathbf{P}\right|^{1/2}} e^{\left(-\frac{\mathbf{x}^T\mathbf{P}^{-1}\mathbf{x}}{2}\right)} \tag{2.23}$$

where N is the dimension of the state. The probability density function as a function of number of standard deviations, k is:

$$f(k) = \frac{1}{2^{\frac{N}{2}-1}\Gamma\left(\frac{N}{2}\right)} k^{N-1} e^{\left(-\frac{k^2}{2}\right)} \tag{2.24}$$

The Gamma function $\Gamma\left(x\right)$ is given by:

$$\Gamma\left(x\right) = \int_0^\infty u^{x-1}e^{-u}du \tag{2.25}$$

The probability distribution function as a function of k is then given by:

$$F(k) = \frac{1}{2^{\frac{N}{2}-1}\Gamma\left(\frac{N}{2}\right)} \int_0^k r^{N-1} e^{\left(-\frac{k^2}{2}\right)} dr \tag{2.26}$$

For our purposes N=2. The theoretical probability density function and probability distribution function for a two dimensional system are:

$$\begin{aligned} f(k) &= ke^{\frac{-k^2}{2}} \\ F(k) &= 1 - e^{\frac{-k^2}{2}} \end{aligned} \tag{2.27}$$

2. Probability Distribution Results

For the probability distribution, five evenly spaced points were investigated over a range of uncertainty of the normalized semi-major axis. The range used for this analysis is $1\text{x}10^{-4}$ to $3\text{x}10^{-3}$ corresponding to a range of semi-major axis uncertainty of 0.7 km to 21 km. This is summarized in Table 3. Initially the uncertainty in mean anomaly is left at 0.01° through the range of semi-major axis uncertainty.

Range of Uncertainty in Normalized Semi-Major Axis					
$\sigma_{\delta a^*}$	$1.000\text{x}10^{-4}$	$8.250\text{x}10^{-4}$	$1.550\text{x}10^{-3}$	$2.275\text{x}10^{-3}$	$3.000\text{x}10^{-3}$

Table 3. Normalized Semi-Major Axis

Given Equation (2.27), at k=3 for the theoretical linear system, *F(k)* is 0.9889. That is, a 2D system at 3σ standard deviation should theoretically capture 98.9% of the distribution. In Table 4, the data presented shows the value of k when 98.9% of the distribution is captured for each of the methods of propagation. If the approximation is adequately capturing the dynamics, the k @ 98.9% row should remain close to 3. If it does not, this indicates more standard deviations are required to capture the system dynamics. The values of *F(k)* at k=3 for the first and second-order approximation as well as the exact propagation are is also shown in Table 4. This allows us to evaluate how much the propagation degrades with time.

During this analysis, it was discovered that the $\sigma_{\delta a^*} = 1.0x10^{-4}$ / $\sigma_{\delta M} = 0.01^{\circ}$case showed excellent agreement in the first-order approximation. This is due to the higher order effects being a function of δa^* and the percentage change between the first and second-order approximations being smaller with larger $\sigma_{\delta M}$. The results presented in this section start at $\sigma_{\delta a^*} = 8.25x10^{-4}$ or 5.775 km. The behavior corresponding to the $\sigma_{\delta a^*} = 1.0x10^{-4}$ case will be presented later along with discussion on the relative behavior between $\sigma_{\delta a^*}$ and $\sigma_{\delta M}$.

	Probability Distribution - $\sigma_{\delta a^*}$= 8.25x10^{-4}										
	Orbits	**2**	**4**	**6**	**8**	**10**	**20**	**40**	**60**	**80**	**100**
Linear	*k* @ 98.9%	3.05	3.21	3.51	3.80	4.19	6.51	11.96	17.56	23.30	29.10
	F(k) @ *k*=3	0.987	0.983	0.974	0.964	0.951	0.882	0.770	0.684	0.619	0.569
2nd Order	*k* @ 98.9%	3.04	3.16	3.37	3.54	3.73	4.45	4.91	5.00	5.05	5.07
	F(k) @ *k*=3	0.988	0.985	0.979	0.973	0.967	0.949	0.940	0.937	0.936	0.935
Exact	*k* @ 98.9%	3.06	3.19	3.40	3.59	3.79	4.54	4.95	5.06	5.11	5.13
	F(k) @ *k*=3	0.987	0.984	0.977	0.972	0.966	0.947	0.938	0.934	0.933	0.933

Table 4. Probability Distribution - $\sigma_{\delta a}$ = 5.775 km

One can see in Table 4 that the first-order approximation begins to significantly degrade by 20 orbits. This is further illustrated in Figure 6. The dashed red line represents the theoretical probability distribution from Equation (2.27). The remaining curves are the probability distribution plotted at 20 orbit increments out to 100 orbits. The linear propagation curves flatten out with propagation time. This indicates a larger standard deviation is needed to capture the distribution.

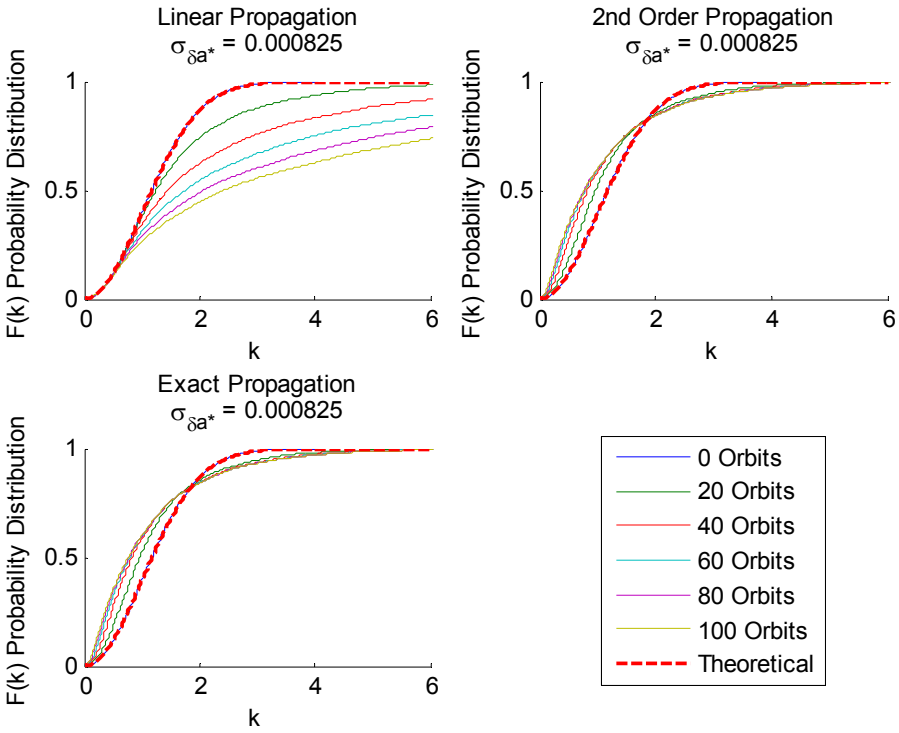

Figure 6. Probability Distribution Comparison, 100 Orbits - $\sigma_{\delta a}$ = 5.775 km

Tables 5 through 7 are the summary of the probability distribution for the remainder of the range of uncertainty in semi-major axis. The remaining probability distribution comparison plots are left for the appendix. It can be seen in Tables 5 through 7 that as we increase the initial uncertainty in semi-major axis, leaving the initial uncertainty in mean anomaly at 0.01°, the accurateness of the first-order approximation decreases.

	Probability Distribution - $\sigma_{\delta a^*}$ = 1.55x10^{-3}										
	Orbits	**2**	**4**	**6**	**8**	**10**	**20**	**40**	**60**	**80**	**100**
Linear	*k* @ 98.9%	3.68	5.11	6.85	8.78	10.71	20.59	40.94	61.40	81.69	102.06
	F(k) @ *k*=3	0.969	0.924	0.875	0.830	0.792	0.646	0.497	0.417	0.367	0.331
2nd Order	*k* @ 98.9%	3.44	4.09	4.51	4.73	4.85	5.02	5.09	5.10	5.10	5.10
	F(k) @ *k*=3	0.976	0.959	0.948	0.943	0.941	0.936	0.935	0.935	0.935	0.935
Exact	*k* @ 98.9%	3.49	4.18	4.59	4.79	4.93	5.08	5.13	5.15	5.13	5.12
	F(k) @ *k*=3	0.974	0.956	0.946	0.941	0.939	0.933	0.932	0.932	0.933	0.933

Table 5. Probability Distribution - $\sigma_{\delta a}$ = 10.85 km

	Probability Distribution - $\sigma_{\delta a^*}$ = 2.275x10^{-3}										
	Orbits	**2**	**4**	**6**	**8**	**10**	**20**	**40**	**60**	**80**	**100**
Linear	*k* @ 98.9%	5.37	9.38	13.61	17.82	22.15	44.14	87.93	131.9	175.6	219.1
	F(k) @ *k*=3	0.916	0.818	0.740	0.682	0.630	0.482	0.355	0.292	0.254	0.226
2nd Order	*k* @ 98.9%	4.16	4.77	4.92	4.99	5.03	5.10	5.10	5.11	5.10	5.09
	F(k) @ *k*=3	0.957	0.942	0.939	0.937	0.936	0.935	0.935	0.935	0.935	0.935
Exact	*k* @ 98.9%	4.26	4.85	5.00	5.06	5.10	5.14	5.13	5.13	5.14	5.13
	F(k) @ *k*=3	0.954	0.940	0.936	0.934	0.933	0.932	0.932	0.933	0.933	0.933

Table 6. Probability Distribution - $\sigma_{\delta a}$ = 15.925 km

Table 7 shows that with an initial uncertainty in the semi-major axis equal to 3x10^{-3} after 2 orbits *F(k)* at *k*=3 has already degraded to 84% indicating that the linear approximation is no longer representing a significant portion of the system dynamics. Figure 7 also illustrates this. In addition to the probability distribution plot, Figure 7 shows the uncertainty ellipsoid propagation for comparison.

	Probability Distribution - $\sigma_{\delta a^*}$ = 3x10^{-3}										
	Orbits	**2**	**4**	**6**	**8**	**10**	**20**	**40**	**60**	**80**	**100**
Linear	*k* @ 98.9%	8.30	15.57	23.07	30.61	38.43	76.44	152.6	228.4	304.2	379.9
	F(k) @ *k*=3	0.842	0.709	0.621	0.556	0.507	0.380	0.271	0.222	0.191	0.173
2nd Order	*k* @ 98.9%	4.70	4.97	5.03	5.07	5.10	5.10	5.09	5.08	5.08	5.08
	F(k) @ *k*=3	0.944	0.938	0.936	0.935	0.935	0.935	0.935	0.935	0.935	0.935
Exact	*k* @ 98.9%	4.74	5.03	5.10	5.14	5.14	5.14	5.13	5.13	5.13	5.13
	F(k) @ *k*=3	0.941	0.935	0.933	0.933	0.932	0.933	0.933	0.933	0.933	0.933

Table 7. Probability Distribution - $\sigma_{\delta a}$ = 21 km

It is noteworthy to see that throughout the entire range of uncertainty in semi-major axis, the second-order approximation is consistent out to 100 orbits and closely matches the exact probability distribution. This indicates that for the two dimensional semi-major axis/mean anomaly state, the second-order approximation is very close to the true system dynamics.

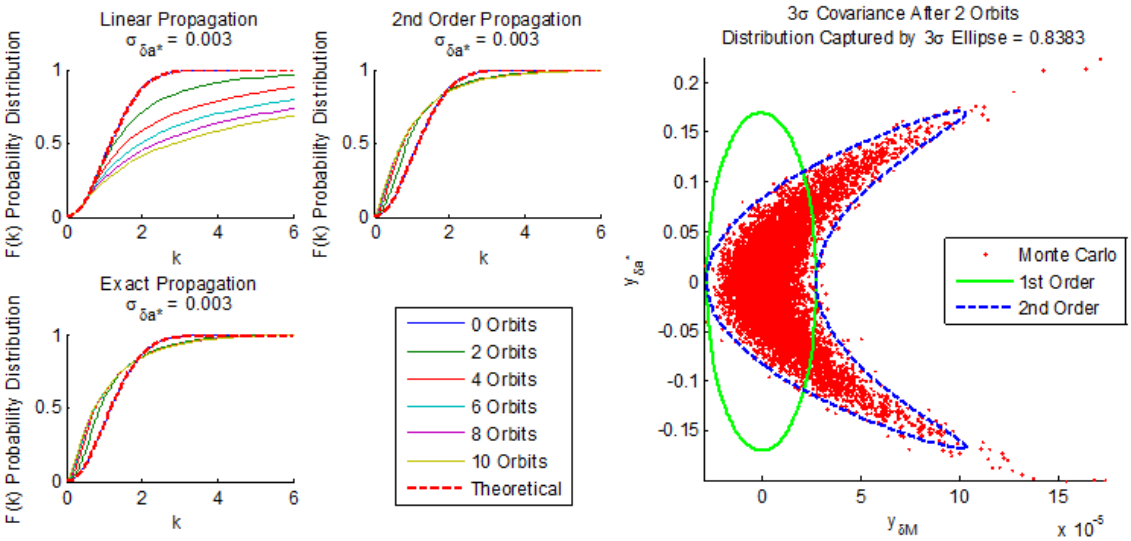

Figure 7. Probability Distribution Comparison, 10 Orbits and Gaussian Distribution Propagated for 2 Orbits - $\sigma_{\delta a} = 21$ km

3. Summary of Probability Distribution

The probability distribution is an excellent way to examine how well a model is fully capturing the dynamics of a system. The results indicate that with larger initial uncertainty in semi-major axis, the first-order approximation fails much quicker than with smaller initial uncertainty.

The results for the $\sigma_{\delta a^*} = 1.0x10^{-4}$ were not presented in this section and are included later in a section that evaluates the relative behavior of $\sigma_{\delta a^*}$ and $\sigma_{\delta M}$. Additionally, only variations in $\sigma_{\delta a^*}$ were presented. The results discussing the relative behavior will show that with a larger initial $\sigma_{\delta M}$ relative to $\sigma_{\delta a^*}$, there is less of a percentage difference between the first-order and higher order solutions.

IV. PERFORMANCE METRICS

A. INTRODUCTION

There has been significant work done in the area of nonlinear performance metrics. This chapter is an examination of previous work in the area of performance metrics of prediction error and uncertainty effects as well as an examination of the relative behavior between initial uncertainty in mean anomaly and semi-major axis. The ultimate goal is to determine if a metric can be developed to predict when ignored nonlinear effects on covariance propagation have rendered an approximation no longer useful.

B. PREDICTION ERROR COST FUNCTION

1. Overview

Horwood, et al. [11] developed a metric for uncertainty consistency called the prediction error to help identify errors in nonlinear and linear propagation techniques. The prediction error is given by:

$$\mathcal{PE}(t) = \int p_1(\mathbf{x},t) p_2(\mathbf{x},t)\, d\mathbf{x} \tag{3.1}$$

where p_1 and p_2 are the probability density functions for two satellite states evaluated at a common time integrated over the entire state space. The cost metric is defined by:

$$c(t) = -\ln \mathcal{PE}(t) \tag{3.2}$$

or

$$c(t) = \frac{1}{2}(\mathbf{x}_1 - \mathbf{x}_2)^T (\mathbf{P}_1 + \mathbf{P}_2)^{-1} (\mathbf{x}_1 - \mathbf{x}_2) + \frac{1}{2}\ln\left[\det\left(2\pi(\mathbf{P}_1 + \mathbf{P}_2)\right)\right] \tag{3.3}$$

The first term in Equation (3.3) is one half of the square of the Mahalanobis distance [12] and the second term is the determinant of the covariance. It will be useful to analyze each of these terms separately:

$$c_1(t) = \frac{1}{2}(\mathbf{x}_1 - \mathbf{x}_2)^T (\mathbf{P}_1 + \mathbf{P}_2)^{-1} (\mathbf{x}_1 - \mathbf{x}_2)$$
$$c_2(t) = \frac{1}{2}\ln\left[\det\left(2\pi(\mathbf{P}_1 + \mathbf{P}_2)\right)\right] \tag{3.4}$$

where the total cost, $c(t) = c_1(t) + c_2(t)$. Additionally, for purposes of this thesis, although unrealistic, we will be using a "truth" orbit for orbit 2. Therefore, the state deviation $\mathbf{x}_2$ and uncertainty $\mathbf{P}_2$ are both zero. Equation (3.4) reduces to:

$$c_1(t) = \frac{1}{2}\mathbf{x}_1^T \mathbf{P}_1^{-1} \mathbf{x}_1$$
$$c_2(t) = \frac{1}{2}\ln\left[\det\left(2\pi\mathbf{P}_1\right)\right] \tag{3.5}$$

with the sum of c_1 and c_2 being the entire cost function. The first term of the cost function uses the Mahalanobis distance, so prior to evaluating the cost function, we will examine the MD with respect to the state.

2. Mahalanobis Distance

The Mahalanobis distance is a way to determine the statistically weighted difference between two points. The Mahalanobis distance is given by:

$$k^2 = \delta\mathbf{x}^T \mathbf{P}^{-1} \delta\mathbf{x},$$
$$\text{where} \tag{3.6}$$
$$\delta\mathbf{x} = \mathbf{x}(t) - \bar{\mathbf{x}}(t)$$

where the "bar" over the state indicates a value on the reference orbit. Recall from Equation (1.13) that $\delta a^* = \delta a_0^*$ and our reference orbit is the truth orbit. Therefore:

$$\delta\mathbf{x} = \begin{bmatrix} a - \bar{a} \\ M(t) - \bar{M}(t) \end{bmatrix} = \begin{bmatrix} \delta a_0 \\ \delta M \end{bmatrix} \tag{3.7}$$

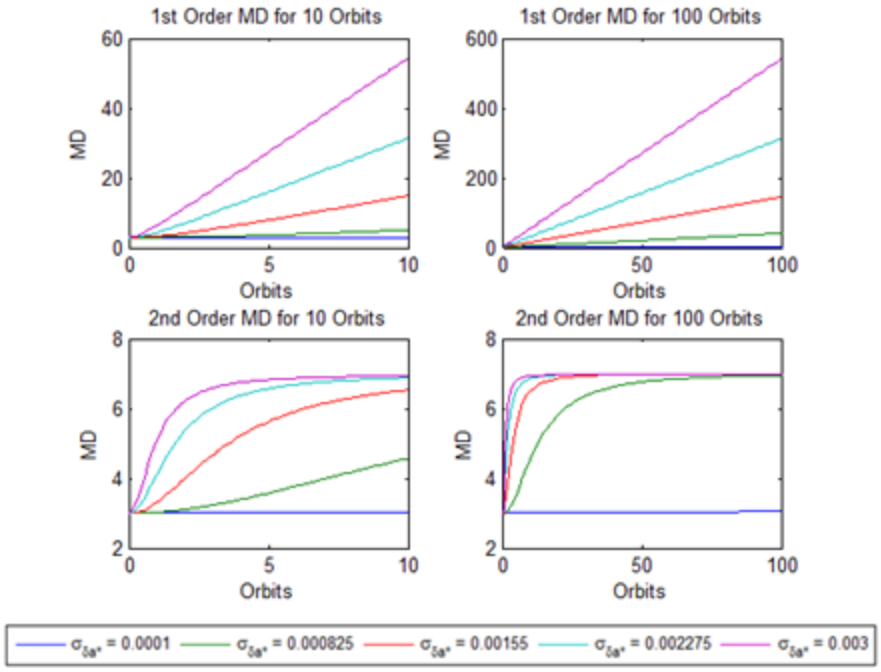

Figure 8. Mahalanobis Distance - First and Second-Order Approximations

The Mahalanobis distance for the first and second-order propagation is plotted in Figure 8. For a linear system, the Mahalanobis distance is constant. Our system is nonlinear but uses approximations to propagate the uncertainty. As one would expect for the initial conditions $\delta a_0^* = 3\sigma_{\delta a^*}$ and $\delta M_0 = 0$ the MD starts at 3 and grows larger with time. For the linear propagation, the MD starts at 3 and grows infinitely large with time. Interestingly, for the second-order approximation, the MD approaches an asymptote. How quickly the second-order MD approaches the asymptotic value is proportional to $\sigma_{\delta a^*}$. Smaller $\sigma_{\delta a^*}$ results in smaller change in MD suggesting the first and second-order approximations show good agreement with the exact propagation. It will be shown later that this is also a function of the relative behavior between initial uncertainty in δa_0^* and δM_0. Overall, the departure of the Mahalanobis distance from the initial value at initial time is a method of indicating how well your approximation is capturing the full nonlinear dynamics.

3. Prediction Error Cost Function Results

The cost function will be used to compare the results of the first and second-order approximations. In order to obtain the initial covariance, we must define our initial uncertainty. The uncertainty in mean anomaly is left at 0.01°. Equation (1.26) shows that it is the uncertainty in the semi-major axis or the radial direction that causes the mean anomaly error or in-track error to grow with time. Due to this, we will consider a range of uncertainties in semi-major axis. To get an accurate comparison with previous results, the non-dimensional semi-major axis uncertainties considered are $1\text{x}10^{-4}$ to $3\text{x}10^{-3}$ corresponding to a range of uncertainty from 0.7 km to 21 km. One can see from Equation (3.3) that the initial cost at time zero is dependent on the selection of the initial conditions. The initial condition used for prediction error cost analysis is $\delta a_0^* = 3\sigma_{\delta a^*}$ and $\delta M_0 = 0$. A different initial condition would result in a different value for initial and final cost and ultimately a different total cost. The choice of initial condition is based $\delta a_0^* = 3\sigma_{\delta a^*}$ being the "worst case" from a range of uncertainty bounded by the 3σ ellipse. The total cost for 10 orbits is plotted in Figure 9.

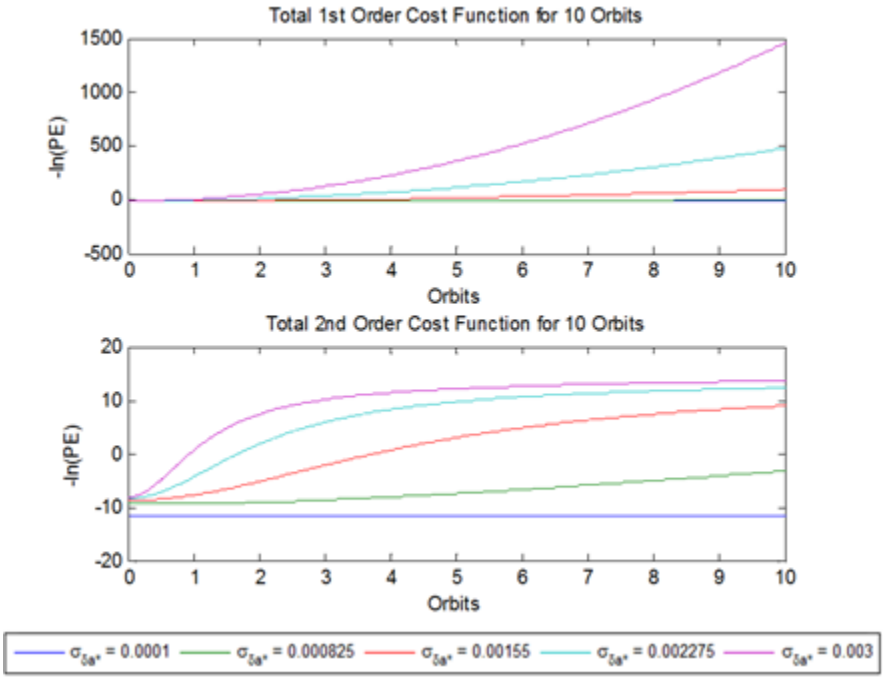

Figure 9. Total Cost Metric for 10 Orbits - First and Second-Order Approximation

The results of the total cost as well as the Mahalanobis distance for the first-order approximations are summarized in Table 8. Propagation times are set at 10 as well as 100 orbits for comparison. Interestingly, for a small initial uncertainty, or $\sigma_{\delta a^*} = 1x10^{-4}$, there is very little change in total cost or MD over both the 10 and 100 orbit propagation times. This initially would indicate that the uncertainty consistency is well represented for smaller $\sigma_{\delta a^*}$. Like the Mahalanobis distance, the performance of the $\sigma_{\delta a^*} = 1x10^{-4}$ case is in reality maximizing performance of the relative behavior between $\sigma_{\delta M}$ and $\sigma_{\delta a^*}$.

The c_2 term of the first-order approximation requires some discussion. The second term of the cost is a function of the determinant of the covariance. Alfriend [1] proved that for Hamiltonian systems, the volume of the uncertainty ellipsoid is constant with time. In other words, the determinant of the covariance is constant. This was also demonstrated during the covariance ellipsoid propagation with the "thinning" of the ellipsoid as it grew in the δM direction. Due to the constant area of the covariance ellipsoid propagated under the first-order approximation, the difference in the c_2 term or the total cost in c_2 over the propagation time is zero.

1st Order Approximation				
10 Orbits				
$\sigma_{\delta a^*}$	**Total Cost**	**Term 1 Cost**	**Term 2 Cost**	**MD**
$1.000x10^{-4}$	$1.8440x10^{-3}$	$1.8440x10^{-3}$	0	3.000615
$8.250x10^{-4}$	8.4991	8.4991	0	5.098846
$1.550x10^{-3}$	105.3632	105.3632	0	14.823173
$2.275\ x10^{-3}$	486.5164	486.5164	0	31.337402
$3.000x10^{-3}$	1463.7658	1463.7658	0	54.189773
100 Orbits				
$\sigma_{\delta a^*}$	**Total Cost**	**Term 1 Cost**	**Term 2 Cost**	**MD**
$1.000x10^{-4}$	0.1844	0.1844	0	3.060849
$8.250x10^{-4}$	849.9114	849.9114	0	41.337911
$1.550x10^{-3}$	$1.0536x10^{4}$	$1.0536x10^{4}$	0	145.195203
$2.275x10^{-3}$	$4.8652x10^{4}$	$4.8652x10^{4}$	0	311.949164
$3.000x10^{-3}$	$1.4638x10^{5}$	$1.4638x10^{5}$	0	541.075005

Table 8. First-Order Approximation Cost and Mahalanobis Distance

The results of the total cost for the second-order approximation are summarized in Table 9. As one would expect, overall the total cost for the first-order approximation is greater than the second-order approximation indicating greater uncertainty consistency with a second-order approximation. However, this does not hold with the $\sigma_{\delta a^*} = 1x10^{-4}$ case. The total cost for this case is very close for the first and second-order approximation. The case with initial uncertainties of $\sigma_{\delta a^*} = 1x10^{-4}$ and $\sigma_{\delta M} = 0.01^\circ$ show good agreement between the first and second-order approximations. This agrees with the results obtained from the probability distribution and is also due to the relative behavior in initial uncertainties.

As stated previously, a property of a linearly propagated covariance is that the volume is constant with time. The term c_2 is simply the volume of the covariance scaled by a constant. The condition of the covariance ellipsoid volume being constant with time does not hold for the second-order approximation. One can see there is a contribution for the Term 2 cost at $\sigma_{\delta a^*} = 1.0x10^{-4}$. This actually results in a slightly higher cost for the second-order approximation for this case.

2nd Order Approximation				
10 Orbits				
$\sigma_{\delta a^*}$	**Total Cost**	**Term 1 Cost**	**Term 2 Cost**	**MD**
1.000x10^{-4}	1.8894x10^{-3}	1.8438x10^{-3}	4.5560x10^{-5}	3.000615
8.250x10^{-4}	6.1524	5.9763	0.1761	4.577401
1.550x10^{-3}	17.7490	16.8319	0.9171	6.531751
2.275 x10^{-3}	20.7644	19.1468	1.6176	6.877041
3.000x10^{-3}	21.7236	19.5661	2.1575	6.937740
100 Orbits				
$\sigma_{\delta a^*}$	**Total Cost**	**Term 1 Cost**	**Term 2 Cost**	**MD**
1.000x10^{-4}	0.1873	0.1827	0.0045	3.060305
8.250x10^{-4}	21.5507	19.6676	1.8831	6.952358
1.550x10^{-3}	23.1276	19.9940	3.1336	6.999144
2.275x10^{-3}	23.8234	19.9231	3.9003	6.989003
3.000x10^{-3}	24.2819	19.8285	4.4534	6.975459

Table 9. Second-Order Approximation Cost and Mahalanobis Distance

4. Summary of Cost Function and Mahalanobis Distance

Both the prediction error and the Mahalanobis distance give comparison between an initial and propagated state. The prediction error takes into account higher order statistics with the c_2 term. Neither metric provides definitive information or give a consistent means of determining when the linear approximation is no longer valid. The prediction error cost function is very useful for determining performance gains when using higher order filters, but overall doesn't answer the problem posed in this thesis.

The Mahalanobis distance gives a statistical difference between an initial point and the same point after propagation. Alfriend [1] has shown that the Mahalanobis distance can be used for uncorrelated track association in a more statistically valid manner. With these methods however, the selection of a specific MD as a metric is a balance between accurate correlations and false correlations. Previous work by Hill et al. [3] suggest a MD of less than 10 can be used for UCT association with a reasonable amount of confidence. There is no definitive total change in MD that identifies when the first-order approximation is no longer valid.

C. UNCERTAINTY METRICS

In addition to the work with prediction error cost functions, there have been other studies into determining metrics to assess and compare performance of higher order propagation techniques. In an attempt to determine if these metrics will reveal any information into the validity of a first-order approximation, we will examine these metrics further.

Park and Scheeres developed a metric to assess the performance of the State Transition Tensor method of mapping uncertainties. It was found that when applied to the state used in this thesis, this metric displayed some singularities close to the initial time, $\tau = 0$. Due to this, it was required to slightly modify the Park and Scheeres metric. The results of the modified metric are presented in this section. To begin, a review of the Park and Scheeres metric is conducted.

1. Park and Scheeres Nonlinearity Metric

The Park and Scheeres [7] local nonlinearity index was proposed to assist with determining the sufficient order of higher-order solutions. This local nonlinearity index is defined as:

$$\eta^m\left(t,t^0\right) \triangleq \sup_{\substack{i=1,\ldots,n \\ k-1,\ldots,N}} \frac{\left|\delta\mathbf{x}_i^m\left(t;\delta\mathbf{x}_k^0,t^0\right)-\delta\mathbf{x}_i^*\left(t;\delta\mathbf{x}_k^0,t^0\right)\right|}{\left|\delta\mathbf{x}_i^*\left(t;\delta\mathbf{x}_k^0,t^0\right)\right|} \tag{3.8}$$

where $\delta\mathbf{x}_i^m$ is the mth order approximation of Equation (1.8), $\delta\mathbf{x}_k^0$ is the kth initial condition for $\delta\mathbf{x}$ chosen from the boundary of the initial confidence region, i.e. on the surface of the $k\sigma$ ellipse, and $\delta\mathbf{x}_i^*$ is the exact solution of Equation (1.8). Einstein's summation notation is used and n is the dimension of the state while N is the number of initial conditions.

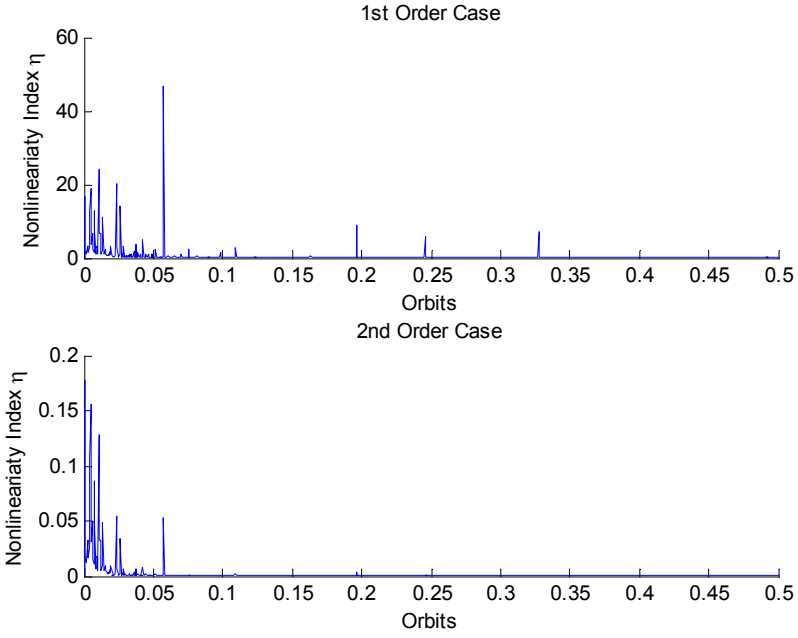

Figure 10. Park and Scheeres Nonlinearity Index

Upon examination of this metric, it was discovered that for the state used in this thesis, there were singularities due to the denominator of Equation (3.8) occasionally

being very close to zero, particularly near time $\tau = 0$. The singularities are illustrated in Figure 10. The results in Figure 10 were obtained using Equation (3.8) with 1000 initial conditions sampled on the 3σ ellipsoid with $\sigma_{\delta a^*} = 0.003$ and $\sigma_{\delta M} = 0.01^\circ$.

The steady state value of η for this particular set of initial conditions and initial uncertainty is actually $1.1255\text{x}10^{-2}$ for the first-order approximation and $1.1823\text{x}10^{-4}$ for the second-order approximation. One can see the singularities at the beginning of the propagation are distorting the curve. The following will derive the limit of the index in order to determine what the steady state behavior is.

Recall that the expression for the exact solution of δM is:

$$\delta M^* = 2\pi\left[\left(a^*\right)^{-3/2} - 1\right]\tau + \delta M_0 \tag{3.9}$$

The Taylor series expansion of $\left(a^*\right)^{-3/2}$ is given by:

$$\begin{aligned} \left(a^*\right)^{-3/2} &= 1 + \sum_{j=1}^{\infty} c_j \left(\delta a^*\right)^j \\ c_j &= \frac{1}{j!}\frac{\partial\left(a^*\right)^{-3/2}}{\partial a^*}\bigg|_{a^*=1} \end{aligned} \tag{3.10}$$

therefore the exact solution for δM becomes:

$$\delta M^* = 2\pi\sum_{j=1}^{\infty} c_j \left(\delta a^*\right)^j \tau + \delta M_0 \tag{3.11}$$

and the *m*th order approximation for the change in mean anomaly is:

$$\delta M^m = 2\pi\sum_{j=1}^{m} c_j \left(\delta a^*\right)^j \tau + \delta M_0 \tag{3.12}$$

The c_j to m=3 are:

$$c_1 = -\frac{3}{2}, \qquad c_2 = \frac{15}{8}, \qquad c_3 = -\frac{105}{48} \tag{3.13}$$

Although the nonlinearity index is a function of the entire state, δa^* is constant. Therefore, only the expression for δM need be considered for the index. Substituting Equation (3.11) and (3.12) into Equation (3.8), the local nonlinearity index becomes:

$$\eta^m\left(t,t^0\right)=\sup_{k=1,\ldots,N}\frac{2\pi\tau\left|\sum_{j=1}^{m}c_j\left(\delta a_k^*\right)^j-\sum_{j=1}^{\infty}c_j\left(\delta a_k^*\right)^j\right|}{\left|2\pi\sum_{j=1}^{\infty}c_j\left(\delta a_k^*\right)^j\tau+\delta M_k^0\right|} \tag{3.14}$$

Consolidating the sigma notation in the numerator gives:

$$\eta^m\left(t,t^0\right)=\sup_{k=1,\ldots,N}\frac{2\pi\tau\left|\sum_{j=m+1}^{\infty}c_j\left(\delta a_k^*\right)^j\right|}{\left|2\pi\sum_{j=1}^{\infty}c_j\left(\delta a_k^*\right)^j\tau+\delta M_k^0\right|} \tag{3.15}$$

With the results in Equation (3.15), there are two observations about the performance of this metric applied to our state. One is that when δM_k^0 and $2\pi\sum_{j=1}^{\infty}c_j\left(\delta a_k^*\right)^j\tau$ are equal and of opposite sign, η^m will be infinite. These singularities often appear near $\tau=0$. Due to this it is necessary to slightly modify the local nonlinearity index. The second observation is that eventually the $\sum_{j=1}^{\infty}c_j\left(\delta a_k^*\right)^j\tau$ term will dominate δM_k^0. Once this occurs, we can express the steady state value reached by Equation (3.15) as:

$$\eta^m\left(t,t^0\right)\approx\sup_{k=1,\ldots,N}\frac{\left|\sum_{j=m+1}^{\infty}c_j\left(\delta a_k^*\right)^j\right|}{\left|\sum_{j=1}^{\infty}c_j\left(\delta a_k^*\right)^j\right|}\approx\sup_{k=1,\ldots,N}\left|\frac{c_{m+1}}{c_1}\left(\delta a_k^*\right)^m\right| \tag{3.16}$$

2. Proposed Performance Index #1

In order to mitigate the singularity behavior with the Park and Scheeres local nonlinearity index, the problem with the term in the denominator being zero needs to be addressed. The first of two proposed performance metrics is given by:

$$\eta^m\left(t,t^0\right) \triangleq \sup_{k-1,\ldots,N} \frac{\left|\delta\mathbf{x}^m\left(t;\delta\mathbf{x}_k^0,t^0\right)-\delta\mathbf{x}^*\left(t;\delta\mathbf{x}_k^0,t^0\right)\right|}{\left|\delta\mathbf{x}^*\left(t;\delta\mathbf{x}_k^0,t^0\right)\right|} \tag{3.17}$$

It is important to note that $\delta\mathbf{x}$ must be dimensionless or each term in $\delta\mathbf{x}$ must have the same dimension. Again, due to the fact that δa^* is constant, we can simplify the expression for η and express it in terms of δM. Equation (3.17) becomes:

$$\eta^m\left(t,t^0\right) \triangleq \sup_{k-1,\ldots,N} \frac{\left|\delta M^m\left(t;\delta\mathbf{x}_k^0,t^0\right)-\delta M^*\left(t;\delta\mathbf{x}_k^0,t^0\right)\right|}{\left[\left(\delta a^*\right)^2+\left(\delta M^*\right)^2\right]^{1/2}} \tag{3.18}$$

Equation (3.18) will start at zero and asymptotically approach the following value:

$$\eta^m\left(\infty,t^0\right) = \sup_{k=1,\ldots,N}\left|\frac{c_{m+1}}{c_1}\left(\delta a_k^*\right)^m\right| \tag{3.19}$$

Consider the $k\sigma_{\delta a^*}$ to be the maximum value of δa^*. This occurs when $\delta M_0 = 0$. This leaves:

$$\eta^m\left(\infty,t^0\right) \approx \left|\frac{c_{m+1}}{c_1}\left(k\sigma_{\delta a^*}\right)^m\right| \tag{3.20}$$

where the c_j come from the Taylor series expansion of $\left(a^*\right)^{-3/2}$ about the reference value $a^* = 1$ given in Equation (3.10).

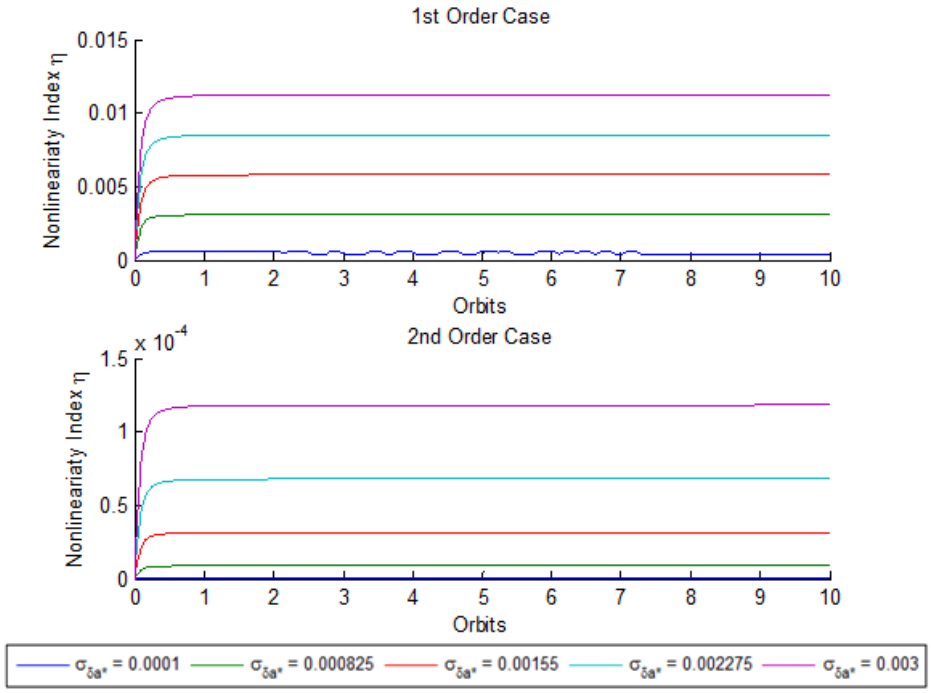

Figure 11. Proposed Performance Metric #1 - 10 Orbits

Figure 10 shows Performance Index #1 for the range of $\sigma_{\delta a^*}$. The uncertainty in mean anomaly is left at 0.01°. One can see that for the $\sigma_{\delta a^*} = 1.0x10^{-4}$ case, the first-order is still showing some discontinuities during initial propagation time and settling on the theoretical value. It is unclear what is causing these discontinuities. Based on the results of this metric, it provides a measure of increased performance with a higher order solution, but does not provide information on when the first-order approximation is no longer valid. Due to this, further investigation into the discontinuities is not warranted.

$\sigma_{\delta a^*}$	$1.000x10^{-4}$	$8.250x10^{-4}$	$1.550x10^{-3}$	$2.275x10^{-3}$	$3.000x10^{-3}$
1st Order Theoretical	$3.7500x10^{-4}$	$3.0937x10^{-3}$	$5.8125x10^{-3}$	$8.5312x10^{-3}$	$1.1250x10^{-2}$
1st Order Numerical	$3.7518x10^{-4}$	$3.0936x10^{-3}$	$5.8134x10^{-3}$	$8.5341x10^{-3}$	$1.1255x10^{-2}$
2nd Order Theoretical	$1.3125x10^{-7}$	$8.9332x10^{-6}$	$3.1532x10^{-5}$	$6.7930x10^{-5}$	$1.1812x10^{-4}$
2nd Order Numerical	$1.3127x10^{-7}$	$8.9338x10^{-6}$	$3.1543x10^{-5}$	$6.7972x10^{-5}$	$1.1823x10^{-4}$

Table 10. Proposed Performance Metric #1 - 10 Orbits

3. Proposed Performance Index #2

The second of the proposed performance metrics relies on the initial uncertainty in mean anomaly. It is given by:

$$\eta^m\left(t,t^0\right) \triangleq \sup_{k-1,\ldots,N} \frac{\left|\delta M^m\left(t;\delta\mathbf{x}_k^0,t^0\right)-\delta M^*\left(t;\delta\mathbf{x}_k^0,t^0\right)\right|}{\left[\left(\delta a^*\right)^2+\left(\delta M_0^*\right)^2\right]^{1/2}} \tag{3.21}$$

Using Equation (3.11) and (3.12), the theoretical behavior for Metric #2 can be expressed analytically in the following manner:

$$\eta^m\left(t,t^0\right) = 2\pi\tau \sup_{k-1,\ldots,N} \frac{\left|\sum_{j=1}^{m} c_j\left(\delta a_k^*\right)^j - \sum_{j=1}^{\infty} c_j\left(\delta a_k^*\right)^j\right|}{\left[\left(\delta a^*\right)^2+\left(\delta M_0^*\right)^2\right]^{1/2}} \tag{3.22}$$

$$\eta^m\left(t,t^0\right) = 2\pi\tau \sup_{k-1,\ldots,N} \frac{2\pi\tau\left|\sum_{j=m+1}^{\infty} c_j\left(\delta a_k^*\right)^j\right|}{\left[\left(\delta a^*\right)^2+\left(\delta M_0^*\right)^2\right]^{1/2}} \tag{3.23}$$

$$\eta^m\left(t,t^0\right) = 2\pi\tau \sup_{k-1,\ldots,N} \frac{\left|c_{m+1}\left(\delta a_k^*\right)^{m+1}\right|}{\left[\left(\delta a^*\right)^2+\left(\delta M_0^*\right)^2\right]^{1/2}} \tag{3.24}$$

Given Equation (3.24) and points selected from the $k\sigma$ ellipsoid, the maximum η^m occurs when $\delta M_0 = 0$ and $\left|\delta a^*\right|$ is a maximum. From Equation (3.24), the theoretical η^m can be expressed analytically as:

$$\eta^m = 2\pi\tau\left|c_{m+1}\left(k\sigma_{\delta a^*}\right)^m\right| \tag{3.25}$$

The numerical results from Equation (3.21) are shown in Figure 12 for 10 orbits. As with previous examples, the range of $\sigma_{\delta a^*}$ is $1\text{x}10^{-4}$ to $3\text{x}10^{-3}$ and $\sigma_{\delta M}$ is 0.01°.

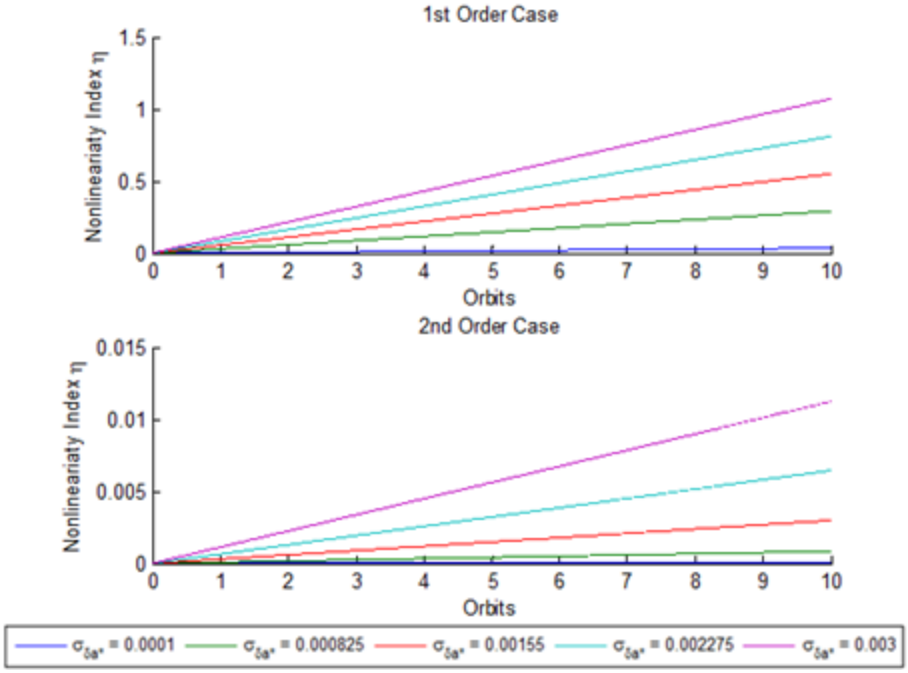

Figure 12. Proposed Performance Metric #2 - 10 Orbits

Table 11 summarizes the results of the numerical versus theoretical comparison for Metric #2. As expected, the total change in the metric is larger for the first-order approximation. One can see there is good agreement between the numerical results obtained through Equation (3.21) and the predicted results from Equation (3.25). Interestingly, the behavior of Metric 2 is consistent throughout the range of uncertainty in δa^* and does not appear to be effected by the relative behavior of initial uncertainties in mean anomaly and semi-major axis.

$\sigma_{\delta a^*}$	$1.000\text{x}10^{-4}$	$8.250\text{x}10^{-4}$	$1.550\text{x}10^{-3}$	$2.275\text{x}10^{-3}$	$3.000\text{x}10^{-3}$
1st Order Theoretical	$3.5343\text{x}10^{-2}$	0.2915	0.5478	0.8040	1.0603
1st Order Numerical	$3.5355\text{x}10^{-2}$	0.2924	0.5507	0.8105	1.0715
2nd Order Theoretical	$1.2370\text{x}10^{-5}$	$8.4193\text{x}10^{-4}$	$2.9719\text{x}10^{-3}$	$6.4023\text{x}10^{-3}$	$1.1133\text{x}10^{-2}$
2nd Order Numerical	$1.2374\text{x}10^{-5}$	$8.4428\text{x}10^{-4}$	$2.9874\text{x}10^{-3}$	$6.4518\text{x}10^{-3}$	$1.1247\text{x}10^{-2}$

Table 11. Proposed Performance Metric #2 - 10 Orbits

4. Summary of Metric Performance

The local nonlinearity index developed by Park and Scheeres was developed to decide the sufficient order of a higher order solution. The original metric as well as Index #1 represent the percent difference between the approximation and the true solution. This is very useful if one defines a threshold of accurateness for an approximation. Ultimately, the metrics do not give definitive information as to when the first-order approximation is no longer representing the system dynamics.

D. RELATIVE BEHAVIOR OF INITIAL UNCERTAINTIES

1. Overview

Thus far it has been suggested that for the $\sigma_{\delta a^*} = 0.0001$ and $\sigma_{\delta M} = 0.01^\circ$ case, there is very good agreement over extended periods of propagation. This prompted further investigation into the relationship between the initial semi-major axis uncertainty and the mean anomaly.

This section will examine the relative behavior between the initial uncertainties and the higher order effects on δM. Additionally, a performance metric is presented that predicts how long the linear approximation is valid given a target distribution and initial uncertainties.

2. First-order Approximation at Small Initial Uncertainty

Figure 13 shows the initial distribution of 10^6 sample points propagated using the complete system dynamics, and then the 3σ uncertainty ellipse propagated using the first and second-order approximations (green ellipse and blue ellipse respectively). At 100 orbits, there is very little difference between the first and second-order approximations and the first-order approximation still encapsulates nearly 99% of the initial distribution. The initial 3σ ellipse for the simulation captured 99.92% of the 10^6 points. MATLAB's pseudorandom number function randn() was used to generate the initial distribution. One can see that even after 100 orbits, the linear approximation identified by the green 3σ ellipse is representing the true system dynamics fairly well. The blue ellipse, which is

slightly distorted, is the second-order approximation, but overall there is very little difference.

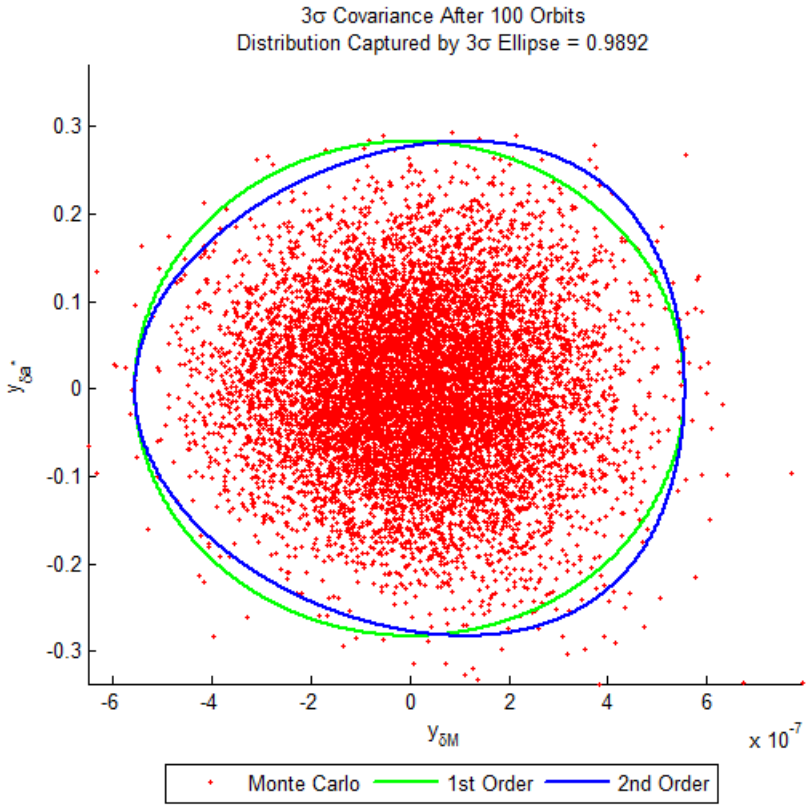

Figure 13. 3σ Uncertainty Ellipse and Gaussian Distribution Propagated for 100 Orbits - $\sigma_{\delta a} = 0.7$ km

Likewise, Figure 14 shows the probability distribution curve using the same initial uncertainty in semi-major axis. At 100 orbits, there is near perfect agreement in first-order, second-order and exact propagations. Table 12 summarizes the results for the probability distribution out to 100 orbits.

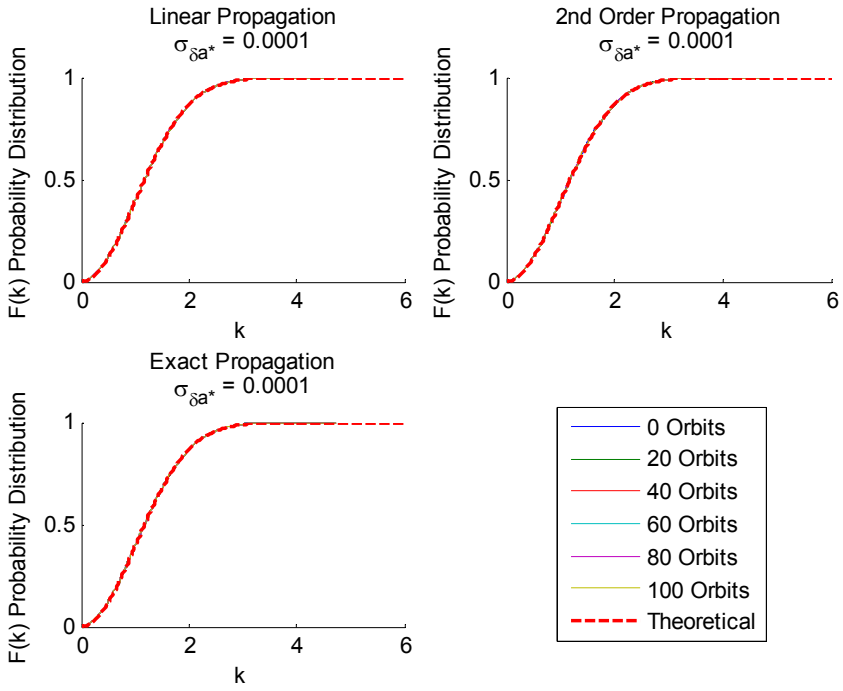

Figure 14. Probability Distribution Comparison, 100 Orbits - $\sigma_{\delta a}$ = 0.7 km

	Probability Distribution $\sigma_{\delta a^*}$ = 0.0001										
	Orbits	**2**	**4**	**6**	**8**	**10**	**20**	**40**	**60**	**80**	**100**
Linear	*k* @ 98.9%	2.99	2.99	2.99	3.00	3.00	3.00	3.01	3.00	3.00	3.02
	F(k) @ *k*=3	0.989	0.989	0.989	0.989	0.989	0.989	0.989	0.989	0.989	0.988
2nd Order	*k* @ 98.9%	2.99	2.99	2.99	3.00	3.00	3.00	3.01	3.00	3.00	3.01
	F(k) @ *k*=3	0.989	0.989	0.989	0.989	0.989	0.989	0.989	0.989	0.989	0.988
Exact	*k* @ 98.9%	3.02	3.02	3.02	3.03	3.03	3.03	3.03	3.03	3.03	3.05
	F(k) @ *k*=3	0.988	0.988	0.988	0.988	0.988	0.988	0.988	0.988	0.987	0.987

Table 12. Probability Distribution - $\sigma_{\delta a}$ = 0.7 km

Finally, looking at the results of the Horwood Prediction Error Cost Function, the Mahalanobis distance, and the performance indices #1 and #2, all of these metrics suggest that the $\sigma_{\delta a^*} = 0.0001$ case, there is excellent agreement between first-order approximations.

Initially, given that the equations of motion are a function of semi-major axis, it seems intuitive that with smaller initial uncertainty in semi-major axis, the first-order

approximation would remain valid for longer propagation time. However, the results at the $\sigma_{\delta a^*} = 0.0001$ / $\sigma_{\delta M} = 0.001^\circ$ case show the first-order approximation captures the system dynamics out to extremely extended propagation times, past even 1000 orbits. Interestingly it was found that if the initial mean anomaly uncertainty was varied so that it was much smaller than the initial uncertainty in semi-major axis, the validity of the approximation was not as good at extended orbital periods.

Figure 15 shows the probability distribution as well as the covariance propagation out to 100 orbits using $\sigma_{\delta a^*} = 0.0001$. The uncertainty in mean anomaly however is changed from the original 0.01° to $\sigma_{\delta M} = 0.001^\circ$. There is still fairly good agreement at 100 orbits, but not as good as the $\sigma_{\delta M} = 0.01^\circ$ case. The right of Figure 15 shows approximately 92% of the distribution captured by the first-order approximation at 100 orbits versus 98.9% at 100 orbits for $\sigma_{\delta M} = 0.01^\circ$. This suggests that the validity of the first-order approximation is a function of the initial mean anomaly uncertainty, which was unexpected.

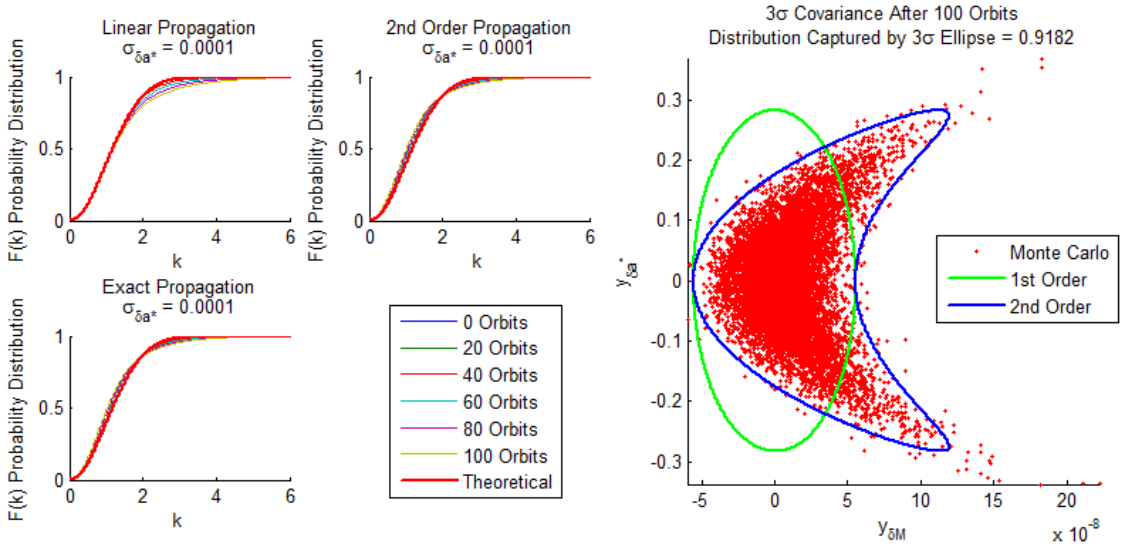

Figure 15. 3σ Uncertainty Ellipse and Gaussian Distribution Propagated for 100 Orbits - $\sigma_{\delta a} = 0.7$ km and $\sigma_{\delta M} = 0.001^\circ$

3. First-order Approximation Error

In this section, a comparison of the first-order approximation and the exact solution is made in order to obtain an expression for the validity of the linear approximation as a function of time and initial uncertainties. In doing so, this will also investigate the relative behavior between initial uncertainty in mean anomaly and semi-major axis and the influence on validity of propagation time.

The exact solution for difference in mean anomaly expressed in non-dimensional terms is:

$$\delta M_{Exact} = 2\pi \left[\sqrt{\frac{1}{\left(1+\delta a^*\right)^3}} - 1 \right] \tau + \delta M_0 \tag{3.26}$$

The first-order approximation is:

$$\delta M_{1st\,Order} = -3\pi \delta a^* \tau + \delta M_0 \tag{3.27}$$

Define γ as the first-order approximation error:

$$\gamma \equiv \delta M_{Exact} - \delta M_{1st\,Order} \tag{3.28}$$

The difference, γ is given by Equation (3.29):

$$\gamma = \left[2\pi \left[\sqrt{\frac{1}{\left(1+\delta a^*\right)^3}} - 1 \right] \tau + \delta M_0 \right] - \left[-3\pi \delta a^* \tau + \delta M_0 \right] \tag{3.29}$$

Simplified, Equation (3.29) becomes:

$$\gamma = \left[\sqrt{\frac{1}{\left(1+\delta a^*\right)^3}} + \frac{3}{2}\delta a^* - 1 \right] 2\pi\tau \tag{3.30}$$

It is notable that Equation (3.30) is not a function of δM_0. This is inconsistent with previous results. In particular, Figures 13 through 15 suggest the initial uncertainty in δM_0 can have a significant influence on the first-order to exact solution error.

Figure 16 shows γ at 1000 orbits for a δa range of ±60 km (60 km representing the approximate 3σ upper bound for δa presented thus far in the thesis). A significant observation from Equation (3.30) and Figure 16 is that when $\delta a = 0$ then $\gamma = 0$. The fact that the first-order approximation error is proportional to δa^* is a contributing factor to why the results thus far show good agreement for the $\delta a^* = 0.0001$. This is only part of the solution, as Equation (3.30) and Figure 16 fail to show any correlation between initial uncertainty in mean anomaly and the first-order approximation validity.

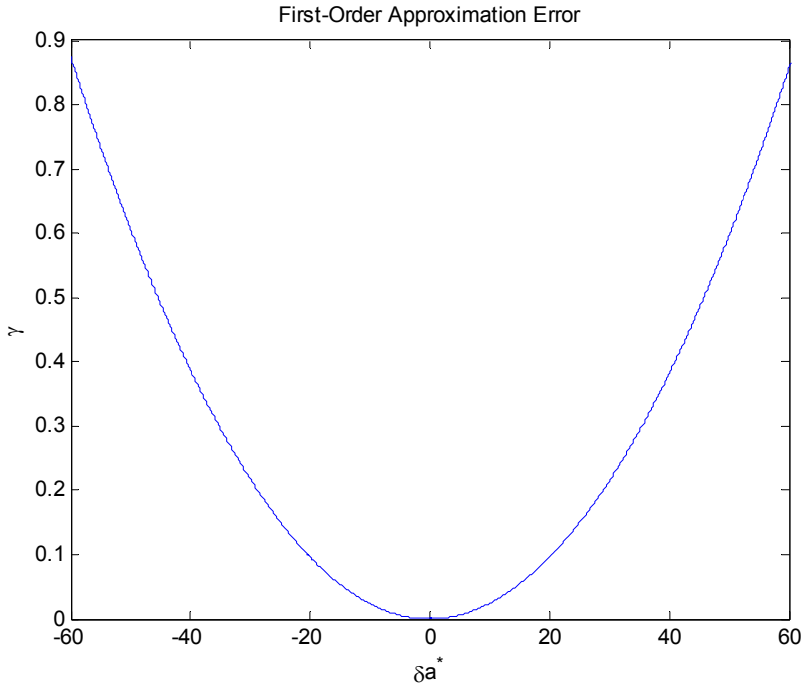

Figure 16. First-Order Approximation Error

4. Linear Approximation Performance Metric

As stated previously, the ultimate goal is to determine if there is a performance metric that can be used to identify when the nonlinearities in the equations of motion

render the first-order approximation invalid. The following is an attempt to analytically relate the validity of the first-order approximation with initial uncertainty in δM_0.

Given that previous results show the validity of the linear approximation is a function of $\sigma_{\delta M_0}$, the $k\sigma$ uncertainties were substituted into Equation (3.30) and γ was set equal to $k\sigma_{\delta M_0}$ in order to determine if this was the time when the linear approximation was no longer capturing the system dynamics.

$$\left[\sqrt{\frac{1}{\left(1+\left(k\sigma_{\delta a^*}\right)\right)^3}}+\frac{3}{2}k\sigma_{\delta a^*}-1\right]2\pi\tau=\left(k\sigma_{\delta M_0}\right) \tag{3.31}$$

Equation (3.31) allows us to obtain a time in terms of number of orbits when the difference between the first-order approximation and exact solution is equal to $k\sigma_{\delta M_0}$. This is given by Equation (3.32)

$$\tau_{k\sigma_{\delta M_0}}=\frac{\left(k\sigma_{\delta M_0}\right)}{\left[\sqrt{\frac{1}{\left(1+\left(k\sigma_{\delta a^*}\right)\right)^3}}+\frac{3}{2}\left(k\sigma_{\delta a^*}\right)-1\right]2\pi} \tag{3.32}$$

Table 13 summarizes the results for k=3 using $\sigma_{\delta M_0}=0.01^\circ$. The same range of initial uncertainties in semi-major axis used throughout this thesis is presented here. Additionally for reference, the probability distribution *F(k)* at $\tau=\tau_{3\sigma_{\delta M_0}}$ is given as well as the value of γ at 1000 orbits.

$\sigma_{\delta a^*}$	$1.000\text{x}10^{-4}$	$8.250\text{x}10^{-4}$	$1.550\text{x}10^{-3}$	$2.275\text{x}10^{-3}$	$3.000\text{x}10^{-3}$
$\tau_{3\sigma_{\delta M_0}}$ (orbits)	494.0	7.276	2.067	0.9617	0.5545
F(k) at $\tau=\tau_{3\sigma_{\delta M_0}}$	0.9681	0.9681	0.9681	0.9681	0.9681
γ at τ=1000 orbits	$1.0599\text{x}10^{-3}$	$7.1958\text{x}10^{-2}$	0.25336	0.54443	0.94434

Table 13. Summary of Performance of $\tau_{3\sigma_{\delta M_0}}$

As shown in Table 13, The first-order approximation *F(k)* is still at approximately 96.8% of the distribution when $3\sigma_{\delta M_0}$ is equal to γ, which is still significant agreement. It follows that setting $k\sigma_{\delta M_0}$ equal to γ does not give the correct metric for assessing the validity of the linear approximation. However, previous results show the validity of the linear approximation is a function of $k\sigma_{\delta M_0}$, so there still is value in examining Equation (3.32).

To further illustrate the behavior of $\tau_{3\sigma_{\delta M_0}}$, Figure 17 shows Equation (3.32) plotted over a range of ±20 km in $\sigma_{\delta a}$. The behavior of $\tau_{3\sigma_{\delta M_0}}$ at $\sigma_{\delta a} = 0$ is infinite; however the y-axis is scaled to 1500 orbits in order to show the relevant behavior. It's clear from Equation (3.32) that with a larger numerator, the behavior of the curves approaching infinity will extend outward, essentially giving a greater number of orbits with larger values of $\sigma_{\delta a}$.

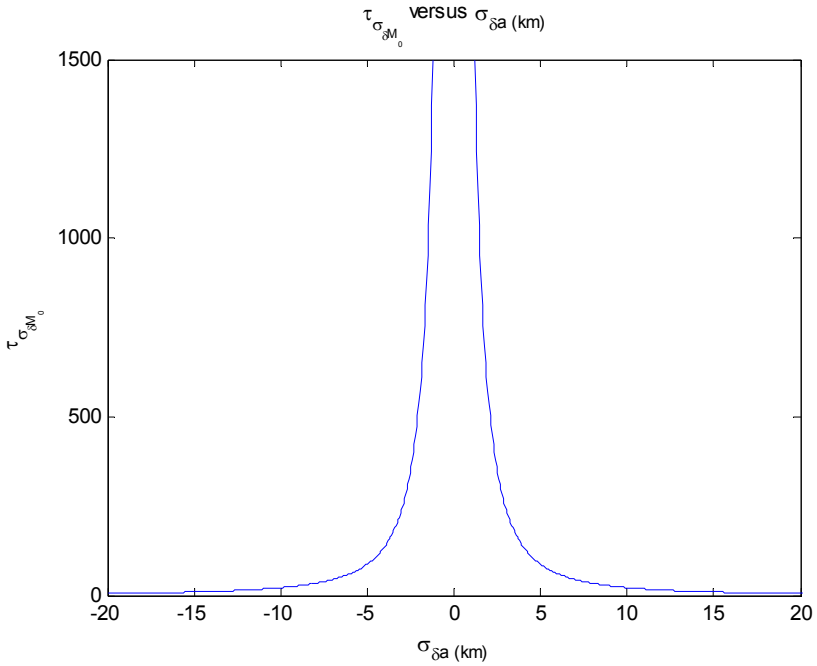

Figure 17. $\tau_{3\sigma_{\delta M_0}}$ with $\sigma_{\delta M_0} = 0.01^\circ$

With respect to the results for Equation (3.32) listed in Table 13, there is interesting behavior with *F(k)*. One can see that the number of orbits obtained change

with different $\sigma_{\delta a}$, but the probability distribution, *F(k)* at $\tau = \tau_{3\sigma_{\delta M_0}}$ does not change with different $\sigma_{\delta a^*}$. Using this property will allow us to determine an expression for the number of orbits as a function of $\sigma_{\delta a^*}$ and $\sigma_{\delta M_0}$ that target a specific percentage of the distribution we want the first-order approximation to capture.

$$\tau_{F(k)} \approx \frac{x\left(k\sigma_{\delta M_0}\right)}{\left[\sqrt{\frac{1}{\left(1+\left(k\sigma_{\delta a^*}\right)\right)^3}}+\frac{3}{2}\left(k\sigma_{\delta a^*}\right)-1\right]2\pi} \tag{3.33}$$

Given values for $\sigma_{\delta a^*}$ and $\sigma_{\delta M_0}$, the number of orbits for a target distribution can be determined experimentally using either the error ellipse propagation or the probability distribution calculation. Equation (3.33) can then be solved for the coefficient *x*. We can then use Equation (3.33) to determine the approximate number of orbits the first-order approximation is good for with a given a target distribution, as a function of $\sigma_{\delta a^*}$ and $\sigma_{\delta M_0}$. A summary of the coefficient, *x* for various target distributions is listed in Table 14.

Target Distribution	0.95	0.9	0.85	0.8	0.75	0.7	0.65
Coefficient	1.35020	2.35425	3.36235	4.46964	5.75911	7.29757	9.15385

Table 14. Summary of Coefficients used for Equation (3.33)

Ultimately the relative performance of the first-order approximation with respect to $\sigma_{\delta M_0}$ is due to the percentage difference from the higher order effects. The mean anomaly error, as well as any higher order contributions to mean anomaly error, are solely a function of δa^*. The first-order approximation for the uncertainty propagation has excellent agreement with the second-order and exact solution at $\sigma_{\delta a^*} = 0.0001$ and $\sigma_{\delta M} = 0.01^\circ$ because the higher order contribution from δa^* is very small relative to $\sigma_{\delta M}$.

THIS PAGE INTENTIONALLY LEFT BLANK

V. CONCLUSIONS

A. KEY POINTS AND RECOMMENDATIONS

In general, it was proven difficult to determine a definitive measure of when the covariance propagated using a linear approximation was no longer Gaussian. The cumulative distribution comparisons allow one to assess the performance of the approximation given initial uncertainty. The propagation of the covariance ellipsoid along with the Monte Carlo simulations provides a good method of visualizing the performance. Using these methods however, much like using the Mahalanobis distance, relies on the user to define a threshold that is no longer acceptable.

The metrics such as the prediction error cost function and the local nonlinearity index provide a way of assessing the significant order of a higher order solution's ability to fully capture a system's dynamics. These metrics however did not provide any information on which initial uncertainties and their size cause propagated covariance to become non-Gaussian.

The performance of the linear approximation with small initial uncertainty in $\sigma_{\delta a^*}$ prompted investigation into the relative behavior between the initial uncertainties. This revealed that although the higher order effects are a function of δa^*, they only have a significant impact when they are large in comparison to the uncertainty ellipse minor axis, which is a function of the initial uncertainty in mean anomaly. During the investigation into the relative behaviors, a linear approximation performance metric was developed. Although it is only applicable to the state as defined in this thesis, a similar approach could be used with a more complex model.

B. AREAS OF FURTHER RESEARCH

The system used in this thesis is very basic, consisting of only two-body motion in the semi-major axis/mean anomaly state space. Previous work referenced throughout this thesis has shown that different coordinate systems can produce vastly different results with respect to nonlinear behavior in first-order approximations. Further research

using different coordinate systems as well as using more complex models is warranted. Additionally, the linear approximation performance metric developed in this thesis could be modified to be made applicable to a real-world model and be used to predict more definitively how long a linear approximation is valid.

APPENDIX A. COVARIANCE EXPANSION TO SECOND-ORDER

$$P_{ij} = \phi_{i,a}\phi_{j,\alpha}P^0_{a\alpha} - \delta m_i \delta m_j + \frac{1}{4}\phi_{i,ab}\phi_{j,\alpha\beta}\left(P^0_{ab}P^0_{\alpha\beta} + P^0_{a\alpha}P^0_{b\beta} + P^0_{a\beta}P^0_{b\alpha}\right)$$

$$P_{11} = \phi_{1,1}\phi_{1,1}P^0_{11} + \phi_{1,1}\phi_{1,2}P^0_{12} + \phi_{1,2}\phi_{1,1}P^0_{21} + \phi_{1,2}\phi_{1,2}P^0_{22} - \delta m_1 \delta m_1 + \frac{1}{4}\begin{bmatrix}
\phi_{1,11}\phi_{1,11}\left(P^0_{11}P^0_{11} + P^0_{11}P^0_{11} + P^0_{11}P^0_{11}\right) + \phi_{1,11}\phi_{1,12}\left(P^0_{11}P^0_{12} + P^0_{11}P^0_{12} + P^0_{12}P^0_{11}\right) + \ldots \\
\phi_{1,11}\phi_{1,21}\left(P^0_{11}P^0_{21} + P^0_{12}P^0_{11} + P^0_{11}P^0_{12}\right) + \phi_{1,11}\phi_{1,22}\left(P^0_{11}P^0_{22} + P^0_{12}P^0_{12} + P^0_{12}P^0_{12}\right) + \ldots \\
\phi_{1,12}\phi_{1,11}\left(P^0_{12}P^0_{11} + P^0_{11}P^0_{21} + P^0_{11}P^0_{21}\right) + \phi_{1,12}\phi_{1,12}\left(P^0_{12}P^0_{12} + P^0_{11}P^0_{22} + P^0_{12}P^0_{21}\right) + \ldots \\
\phi_{1,12}\phi_{1,21}\left(P^0_{12}P^0_{21} + P^0_{12}P^0_{21} + P^0_{11}P^0_{22}\right) + \phi_{1,12}\phi_{1,22}\left(P^0_{12}P^0_{22} + P^0_{12}P^0_{22} + P^0_{12}P^0_{22}\right) + \ldots \\
\phi_{1,21}\phi_{1,11}\left(P^0_{21}P^0_{11} + P^0_{21}P^0_{11} + P^0_{21}P^0_{11}\right) + \phi_{1,21}\phi_{1,12}\left(P^0_{21}P^0_{12} + P^0_{21}P^0_{12} + P^0_{22}P^0_{11}\right) + \ldots \\
\phi_{1,21}\phi_{1,21}\left(P^0_{21}P^0_{21} + P^0_{22}P^0_{11} + P^0_{21}P^0_{12}\right) + \phi_{1,21}\phi_{1,22}\left(P^0_{21}P^0_{22} + P^0_{22}P^0_{12} + P^0_{22}P^0_{12}\right) + \ldots \\
\phi_{1,22}\phi_{1,11}\left(P^0_{22}P^0_{11} + P^0_{21}P^0_{21} + P^0_{21}P^0_{21}\right) + \phi_{1,22}\phi_{1,12}\left(P^0_{22}P^0_{12} + P^0_{21}P^0_{22} + P^0_{22}P^0_{21}\right) + \ldots \\
\phi_{1,22}\phi_{1,21}\left(P^0_{22}P^0_{21} + P^0_{22}P^0_{21} + P^0_{21}P^0_{22}\right) + \phi_{1,22}\phi_{1,22}\left(P^0_{22}P^0_{22} + P^0_{22}P^0_{22} + P^0_{22}P^0_{22}\right)
\end{bmatrix}$$

$$P_{12} = \phi_{1,1}\phi_{2,1}P^0_{11} + \phi_{1,1}\phi_{2,2}P^0_{12} + \phi_{1,2}\phi_{2,1}P^0_{21} + \phi_{1,2}\phi_{2,2}P^0_{22} - \delta m_1 \delta m_2 + \frac{1}{4}\begin{bmatrix}
\phi_{1,11}\phi_{2,11}\left(P^0_{11}P^0_{11} + P^0_{11}P^0_{11} + P^0_{11}P^0_{11}\right) + \phi_{1,11}\phi_{2,12}\left(P^0_{11}P^0_{12} + P^0_{11}P^0_{12} + P^0_{12}P^0_{11}\right) + \ldots \\
\phi_{1,11}\phi_{2,21}\left(P^0_{11}P^0_{21} + P^0_{12}P^0_{11} + P^0_{11}P^0_{12}\right) + \phi_{1,11}\phi_{2,22}\left(P^0_{11}P^0_{22} + P^0_{12}P^0_{12} + P^0_{12}P^0_{12}\right) + \ldots \\
\phi_{1,12}\phi_{2,11}\left(P^0_{12}P^0_{11} + P^0_{11}P^0_{21} + P^0_{11}P^0_{21}\right) + \phi_{1,12}\phi_{2,12}\left(P^0_{12}P^0_{12} + P^0_{11}P^0_{22} + P^0_{12}P^0_{21}\right) + \ldots \\
\phi_{1,12}\phi_{2,21}\left(P^0_{12}P^0_{21} + P^0_{12}P^0_{21} + P^0_{11}P^0_{22}\right) + \phi_{1,12}\phi_{2,22}\left(P^0_{12}P^0_{22} + P^0_{12}P^0_{22} + P^0_{12}P^0_{22}\right) + \ldots \\
\phi_{1,21}\phi_{2,11}\left(P^0_{21}P^0_{11} + P^0_{21}P^0_{11} + P^0_{21}P^0_{11}\right) + \phi_{1,21}\phi_{2,12}\left(P^0_{21}P^0_{12} + P^0_{21}P^0_{12} + P^0_{22}P^0_{11}\right) + \ldots \\
\phi_{1,21}\phi_{2,21}\left(P^0_{21}P^0_{21} + P^0_{22}P^0_{11} + P^0_{21}P^0_{12}\right) + \phi_{1,21}\phi_{2,22}\left(P^0_{21}P^0_{22} + P^0_{22}P^0_{12} + P^0_{22}P^0_{12}\right) + \ldots \\
\phi_{1,22}\phi_{2,11}\left(P^0_{22}P^0_{11} + P^0_{21}P^0_{21} + P^0_{21}P^0_{21}\right) + \phi_{1,22}\phi_{2,12}\left(P^0_{22}P^0_{12} + P^0_{21}P^0_{22} + P^0_{22}P^0_{21}\right) + \ldots \\
\phi_{1,22}\phi_{2,21}\left(P^0_{22}P^0_{21} + P^0_{22}P^0_{21} + P^0_{21}P^0_{22}\right) + \phi_{1,22}\phi_{2,22}\left(P^0_{22}P^0_{22} + P^0_{22}P^0_{22} + P^0_{22}P^0_{22}\right)
\end{bmatrix}$$

$$P_{21} = \phi_{2,1}\phi_{1,1}P^0_{11} + \phi_{2,1}\phi_{1,2}P^0_{12} + \phi_{2,2}\phi_{1,1}P^0_{21} + \phi_{2,2}\phi_{1,2}P^0_{22} - \delta m_2 \delta m_1 + \frac{1}{4}\begin{bmatrix}
\phi_{2,11}\phi_{1,11}\left(P^0_{11}P^0_{11} + P^0_{11}P^0_{11} + P^0_{11}P^0_{11}\right) + \phi_{2,11}\phi_{1,12}\left(P^0_{11}P^0_{12} + P^0_{11}P^0_{12} + P^0_{12}P^0_{11}\right) + \ldots \\
\phi_{2,11}\phi_{1,21}\left(P^0_{11}P^0_{21} + P^0_{12}P^0_{11} + P^0_{11}P^0_{12}\right) + \phi_{2,11}\phi_{1,22}\left(P^0_{11}P^0_{22} + P^0_{12}P^0_{12} + P^0_{12}P^0_{12}\right) + \ldots \\
\phi_{2,12}\phi_{1,11}\left(P^0_{12}P^0_{11} + P^0_{11}P^0_{21} + P^0_{11}P^0_{21}\right) + \phi_{2,12}\phi_{1,12}\left(P^0_{12}P^0_{12} + P^0_{11}P^0_{22} + P^0_{12}P^0_{21}\right) + \ldots \\
\phi_{2,12}\phi_{1,21}\left(P^0_{12}P^0_{21} + P^0_{12}P^0_{21} + P^0_{11}P^0_{22}\right) + \phi_{2,12}\phi_{1,22}\left(P^0_{12}P^0_{22} + P^0_{12}P^0_{22} + P^0_{12}P^0_{22}\right) + \ldots \\
\phi_{2,21}\phi_{1,11}\left(P^0_{21}P^0_{11} + P^0_{21}P^0_{11} + P^0_{21}P^0_{11}\right) + \phi_{2,21}\phi_{1,12}\left(P^0_{21}P^0_{12} + P^0_{21}P^0_{12} + P^0_{22}P^0_{11}\right) + \ldots \\
\phi_{2,21}\phi_{1,21}\left(P^0_{21}P^0_{21} + P^0_{22}P^0_{11} + P^0_{21}P^0_{12}\right) + \phi_{2,21}\phi_{1,22}\left(P^0_{21}P^0_{22} + P^0_{22}P^0_{12} + P^0_{22}P^0_{12}\right) + \ldots \\
\phi_{2,22}\phi_{1,11}\left(P^0_{22}P^0_{11} + P^0_{21}P^0_{21} + P^0_{21}P^0_{21}\right) + \phi_{2,22}\phi_{1,12}\left(P^0_{22}P^0_{12} + P^0_{21}P^0_{22} + P^0_{22}P^0_{21}\right) + \ldots \\
\phi_{2,22}\phi_{1,21}\left(P^0_{22}P^0_{21} + P^0_{22}P^0_{21} + P^0_{21}P^0_{22}\right) + \phi_{2,22}\phi_{1,22}\left(P^0_{22}P^0_{22} + P^0_{22}P^0_{22} + P^0_{22}P^0_{22}\right)
\end{bmatrix}$$

$$P_{22} = \phi_{2,1}\phi_{2,1}P^0_{11} + \phi_{2,1}\phi_{2,2}P^0_{12} + \phi_{2,2}\phi_{2,1}P^0_{21} + \phi_{2,2}\phi_{2,2}P^0_{22} - \delta m_2 \delta m_2 + \frac{1}{4}\begin{bmatrix}
\phi_{2,11}\phi_{2,11}\left(P^0_{11}P^0_{11} + P^0_{11}P^0_{11} + P^0_{11}P^0_{11}\right) + \phi_{2,11}\phi_{2,12}\left(P^0_{11}P^0_{12} + P^0_{11}P^0_{12} + P^0_{12}P^0_{11}\right) + \ldots \\
\phi_{2,11}\phi_{2,21}\left(P^0_{11}P^0_{21} + P^0_{12}P^0_{11} + P^0_{11}P^0_{12}\right) + \phi_{2,11}\phi_{2,22}\left(P^0_{11}P^0_{22} + P^0_{12}P^0_{12} + P^0_{12}P^0_{12}\right) + \ldots \\
\phi_{2,12}\phi_{2,11}\left(P^0_{12}P^0_{11} + P^0_{11}P^0_{21} + P^0_{11}P^0_{21}\right) + \phi_{2,12}\phi_{2,12}\left(P^0_{12}P^0_{12} + P^0_{11}P^0_{22} + P^0_{12}P^0_{21}\right) + \ldots \\
\phi_{2,12}\phi_{2,21}\left(P^0_{12}P^0_{21} + P^0_{12}P^0_{21} + P^0_{11}P^0_{22}\right) + \phi_{2,12}\phi_{2,22}\left(P^0_{12}P^0_{22} + P^0_{12}P^0_{22} + P^0_{12}P^0_{22}\right) + \ldots \\
\phi_{2,21}\phi_{2,11}\left(P^0_{21}P^0_{11} + P^0_{21}P^0_{11} + P^0_{21}P^0_{11}\right) + \phi_{2,21}\phi_{2,12}\left(P^0_{21}P^0_{12} + P^0_{21}P^0_{12} + P^0_{22}P^0_{11}\right) + \ldots \\
\phi_{2,21}\phi_{2,21}\left(P^0_{21}P^0_{21} + P^0_{22}P^0_{11} + P^0_{21}P^0_{12}\right) + \phi_{2,21}\phi_{2,22}\left(P^0_{21}P^0_{22} + P^0_{22}P^0_{12} + P^0_{22}P^0_{12}\right) + \ldots \\
\phi_{2,22}\phi_{2,11}\left(P^0_{22}P^0_{11} + P^0_{21}P^0_{21} + P^0_{21}P^0_{21}\right) + \phi_{2,22}\phi_{2,12}\left(P^0_{22}P^0_{12} + P^0_{21}P^0_{22} + P^0_{22}P^0_{21}\right) + \ldots \\
\phi_{2,22}\phi_{2,21}\left(P^0_{22}P^0_{21} + P^0_{22}P^0_{21} + P^0_{21}P^0_{22}\right) + \phi_{2,22}\phi_{2,22}\left(P^0_{22}P^0_{22} + P^0_{22}P^0_{22} + P^0_{22}P^0_{22}\right)
\end{bmatrix}$$

THIS PAGE INTENTIONALLY LEFT BLANK

APPENDIX B. ADDITIONAL PLOTS

1. Additional Cost Function Plots

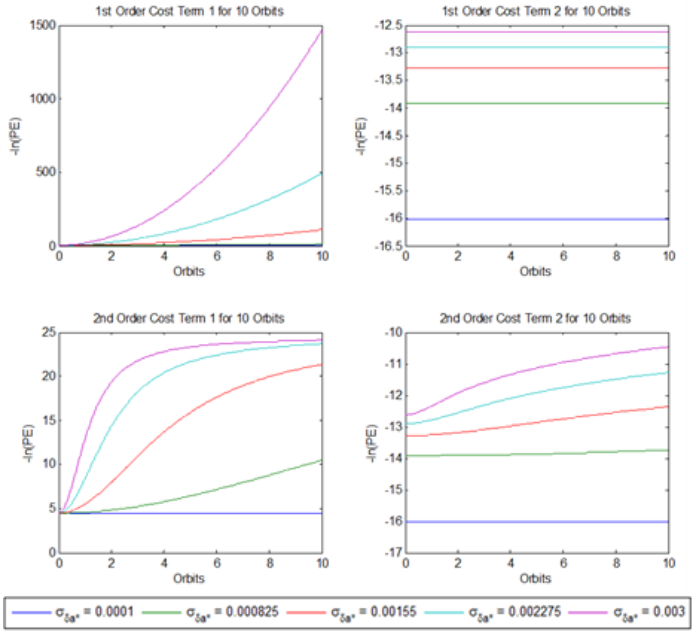

Figure 18. Cost Function Term 1 and 2 for 10 Orbits

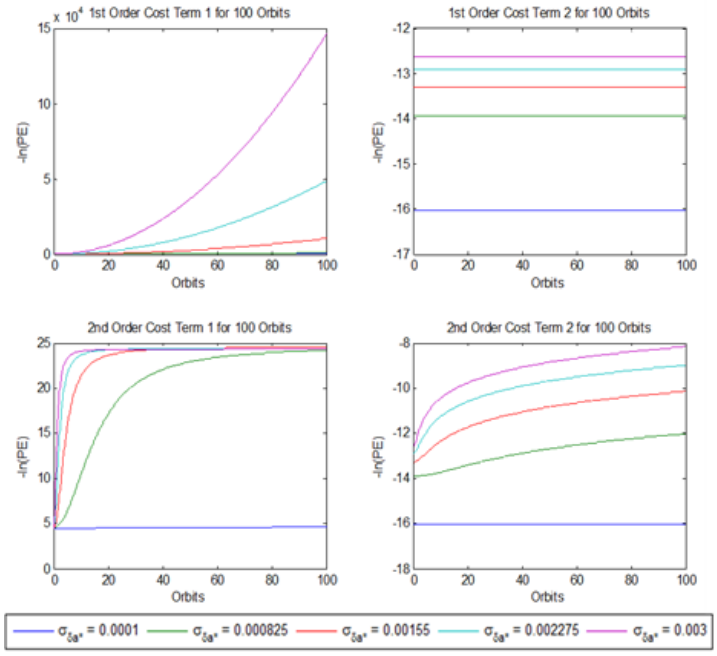

Figure 19. Cost Function Term 1 and 2 for 100 Orbits

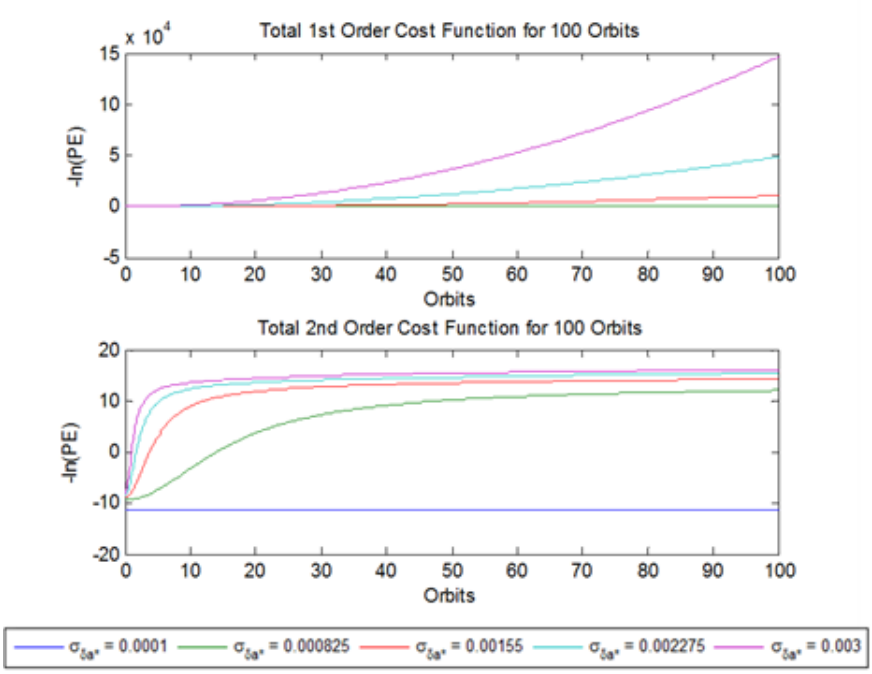

Figure 20. Total Cost Metric for 100 Orbits, First and Second-Order Approximation

2. Additional Probability Distribution Plots

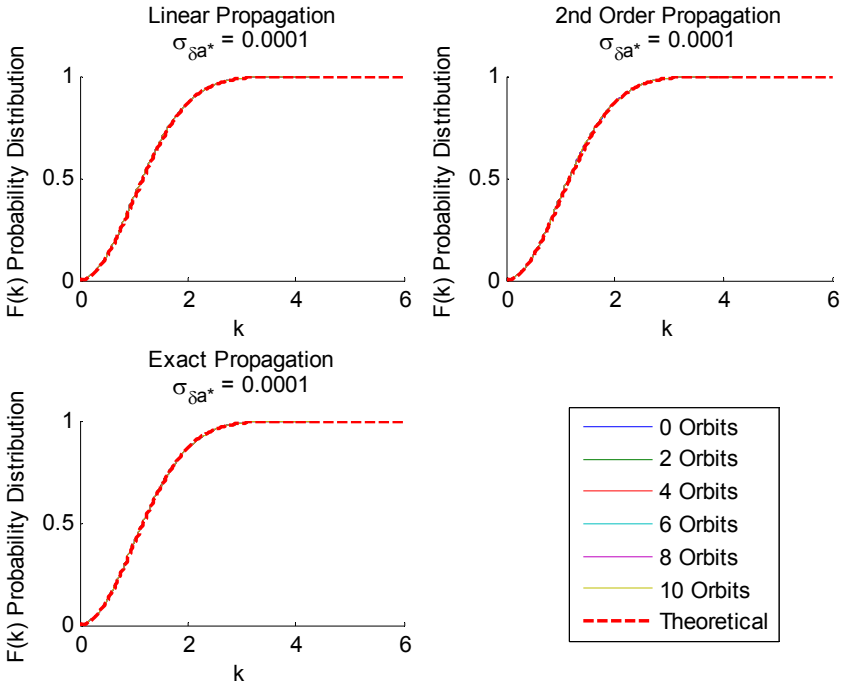

Figure 21. Probability Distribution Comparison, 10 Orbits - $\sigma_{\delta a}$ = 0.7 km

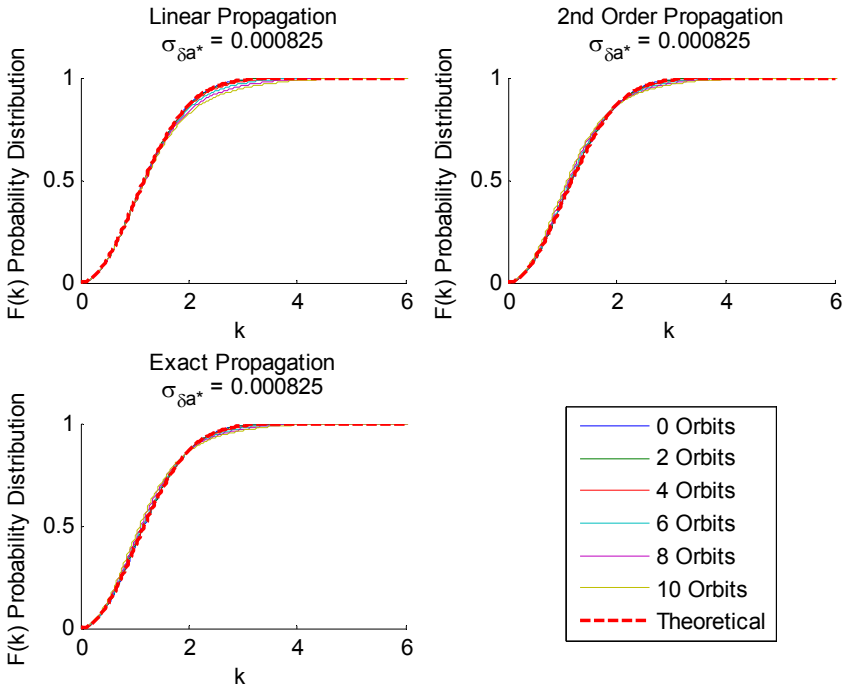

Figure 22. Probability Distribution Comparison, 10 Orbits - $\sigma_{\delta a}$ = 5.775 km

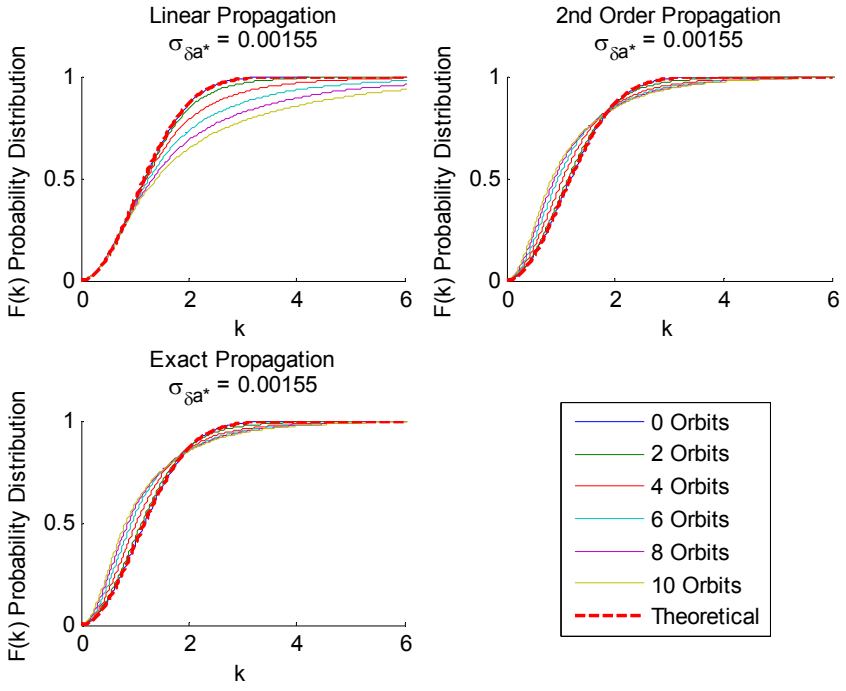

Figure 23. Probability Distribution Comparison, 10 Orbits - $\sigma_{\delta a}$ = 10.85 km

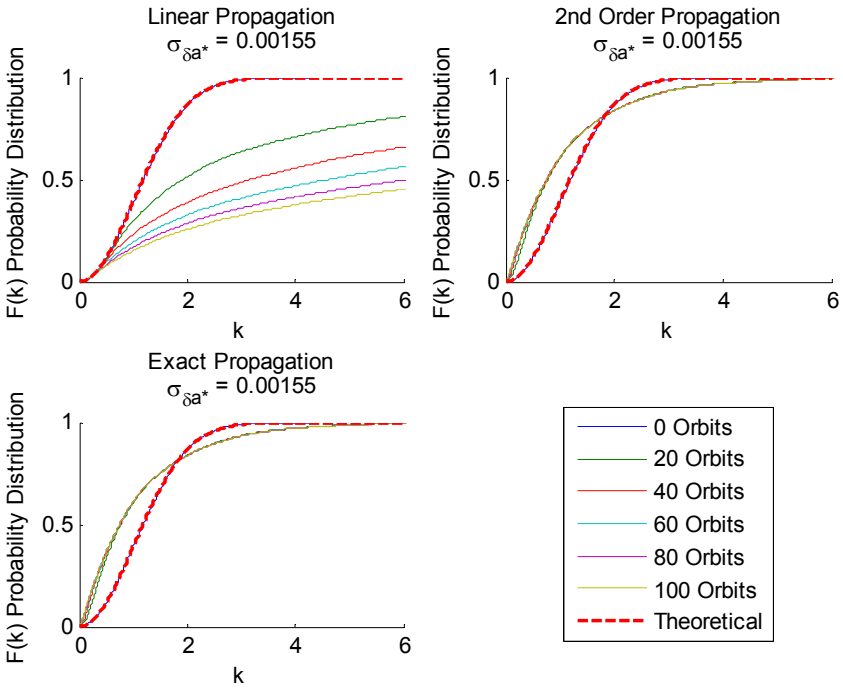

Figure 24. Probability Distribution Comparison, 100 Orbits - $\sigma_{\delta a}$ = 10.85 km

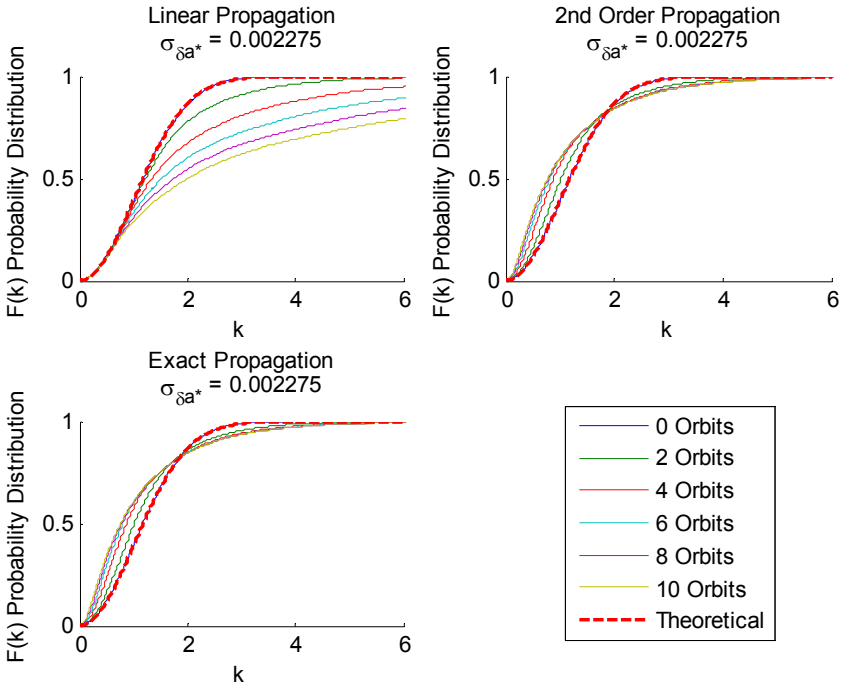

Figure 25. Probability Distribution Comparison, 10 Orbits - $\sigma_{\delta a}$ = 15.925 km

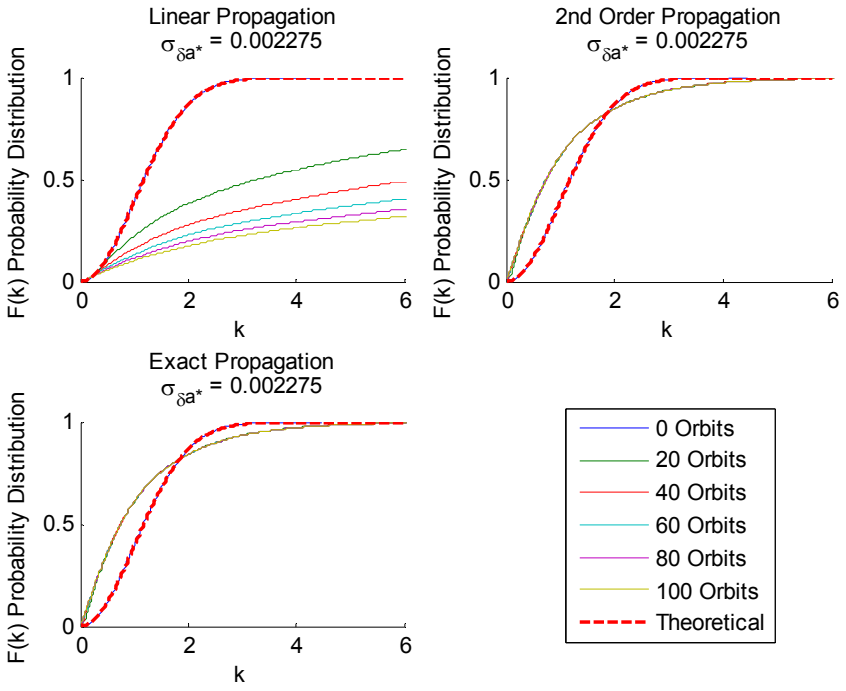

Figure 26. Probability Distribution Comparison, 100 Orbits - $\sigma_{\delta a}$ = 15.925 km

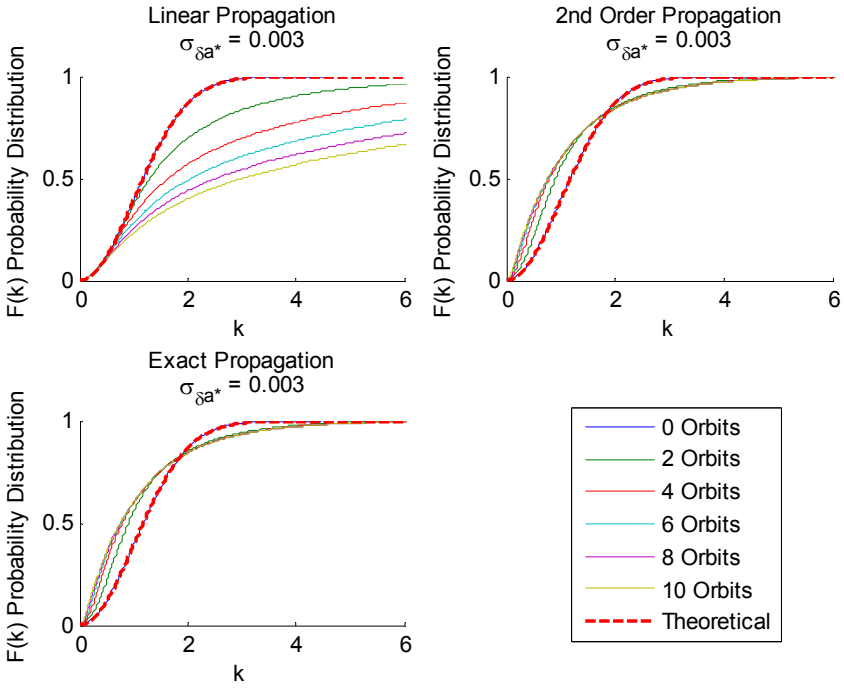

Figure 27. Probability Distribution Comparison, 10 Orbits - $\sigma_{\delta a}$ = 21 km

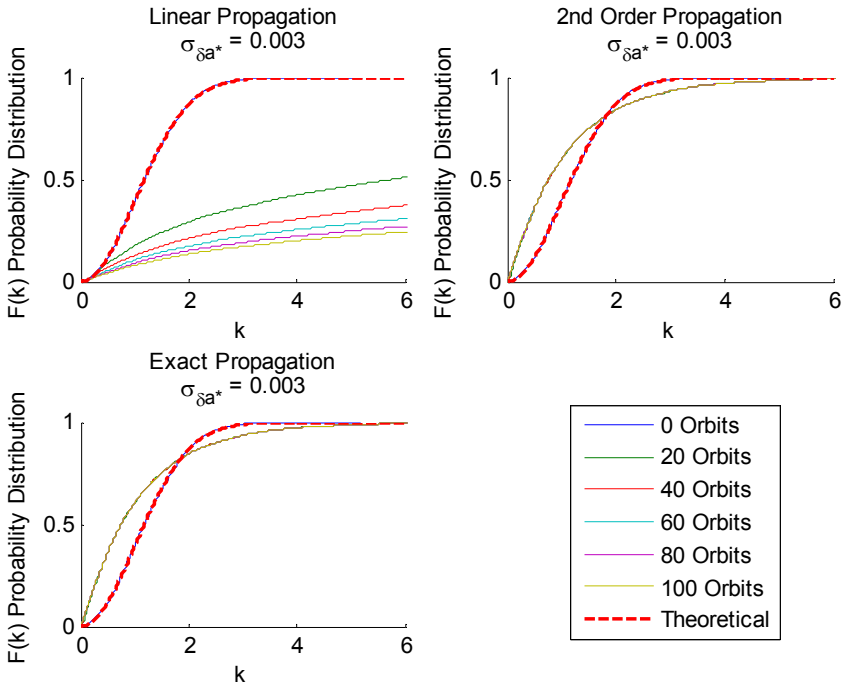

Figure 28. Probability Distribution Comparison, 100 Orbits - $\sigma_{\delta a} = 21$ km

3. Mean Anomaly Error and In-Track Error Plots

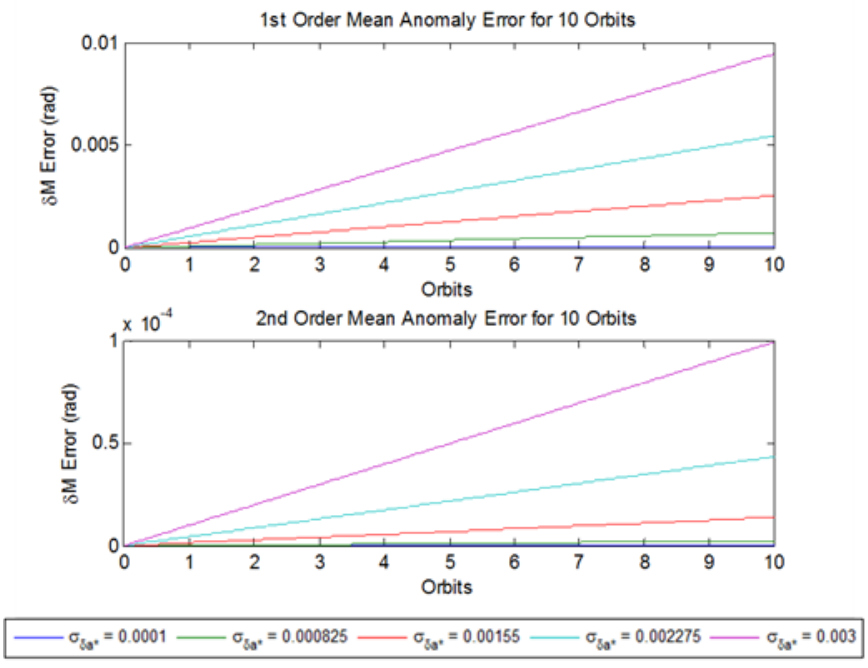

Figure 29. Mean Anomaly Error, 10 Orbits - $\delta a_0^* = 3\sigma_{\delta a^*}$, $\delta M_0 = 0$

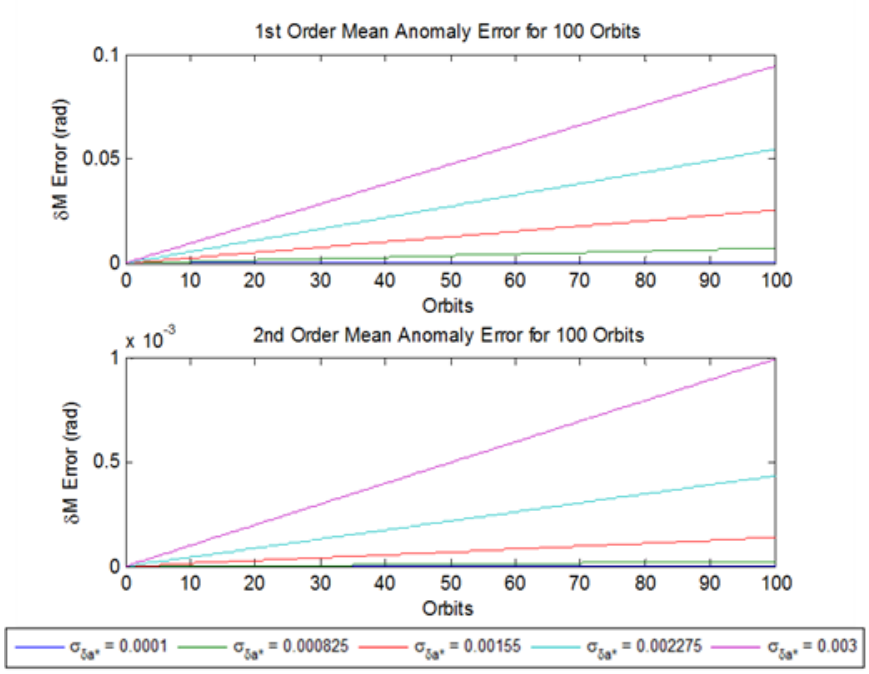

Figure 30. Mean Anomaly Error, 100 Orbits - $\delta a_0^* = 3\sigma_{\delta a^*}$, $\delta M_0 = 0$

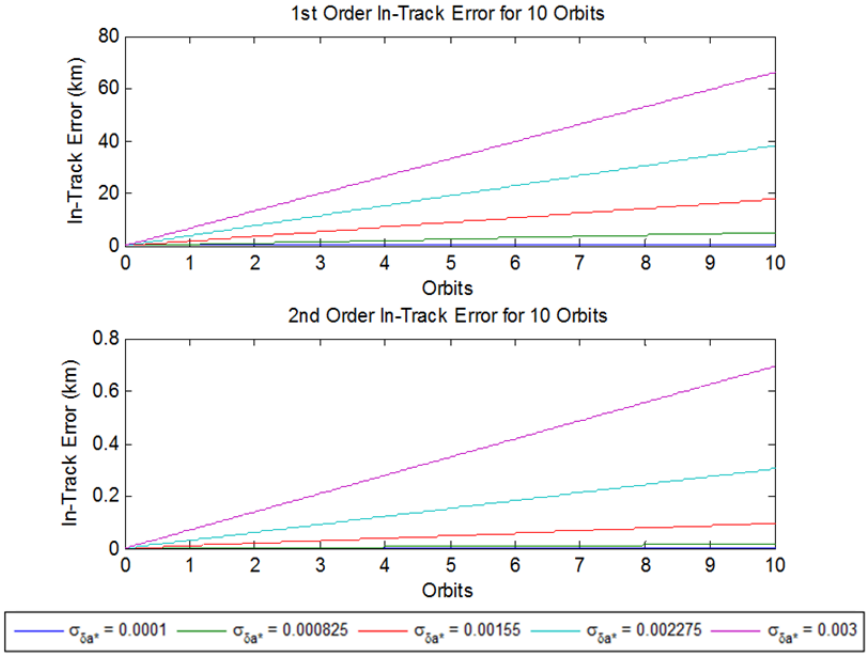

Figure 31. In-Track Error, 10 Orbits - $\delta a_0^* = 3\sigma_{\delta a^*}$, $\delta M_0 = 0$

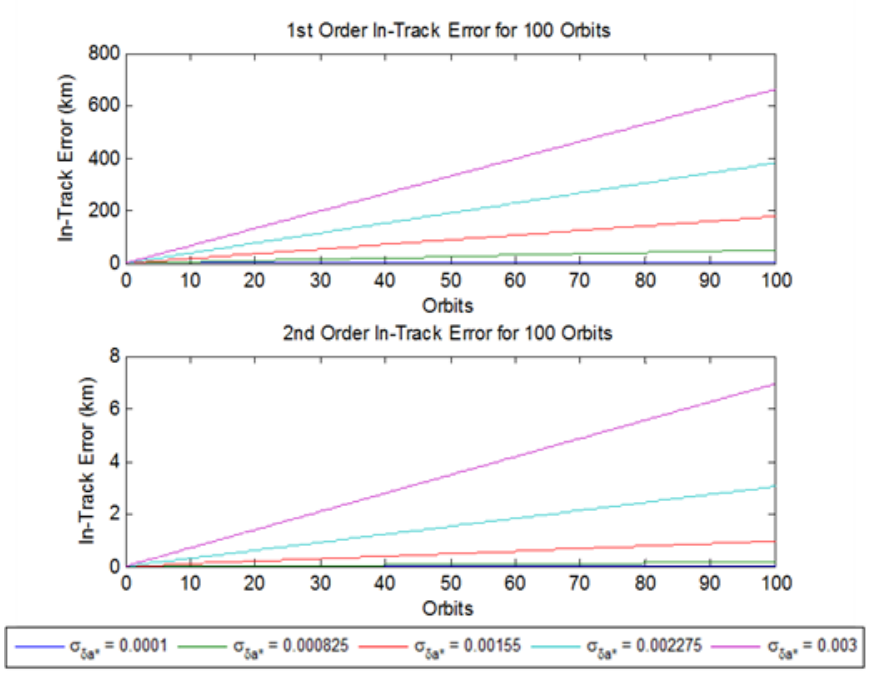

Figure 32. In-Track Error, 100 Orbits - $\delta a_0^* = 3\sigma_{\delta a^*}$, $\delta M_0 = 0$

LIST OF REFERENCES

[1] K. T. Alfriend, "A dynamic algorithm for processing uncorrelated tracks," presented at the 1997 AAS/AIAA Astrodynamics Specialist Conference, Sun Valley, ID, 1997, Paper No. AAS 97-607.

[2] K. Hill *et al*., "Covariance-based uncorrelated track association," presented at the 2008 AIAA/AAS Astrodynamics Conference, Honolulu, HI, 2008, Paper No. AIAA 2008-7211.

[3] K. Hill *et al*., "Comparison of covariance-based track association approaches with simulated radar data," presented at the Kyle T. Alfriend Astrodynamics Symposium, 2010, Paper No. AAS 10-318.

[4] K. T. Alfriend *et al*., "Probability of collision error analysis," *International Journal of Space Debris*, vol. 1, 1999, pp. 21–35

[5] K. Hill *et al*., "Covariance based scheduling of a network of optical sensors," presented at the Kyle T. Alfriend Astrodynamics Symposium, 2010, Paper No. AAS 10-325.

[6] K. Fujimoto *et al*., "Analytical nonlinear propagation of uncertainty in the two-body problem," *Journal of Guidance, Control, and Dynamics*, vol. 35, no. 2, March-April 2012, pp. 497–509.

[7] R. S. Park and D. J. Scheeres, "Nonlinear mapping of Gaussian statistics: Theory and applications to spacecraft trajectory mapping," *Journal of Guidance, Control, and Dynamics,* vol. 29, no. 6, November–December 2006, pp. 1367–1375.

[8] D.W. Gim and K.T. Alfriend, "The state transition matrix of relative motion for the perturbed non-circular reference orbit," *Journal of Guidance, Control, and Dynamics,* vol. 26, no. 6, Nov.–Dec. 2003, pp. 956–971.

[9] J. Prussing and B. Conway, *Orbital Mechanics*. New York, NY: Oxford University Press, 1993.

[10] R. S. Park and D. J. Scheeres, "Nonlinear mapping of Gaussian state covariance and orbit uncertainties," presented at AAS/AIAA Space Flight Mechanics Meeting, Copper Mountain, CO, 2005, Paper No. AAS 05-170.

[11] J. T. Horwood *et al*., "Gaussian sum filters for space surveillance: theory and simulations," *Journal of Guidance, Control, and Dynamics*, vol. 34, no. 6, November–December 2011, pp. 1839–1851.

[12] C. Sabol *et al*., "Linearized orbit covariance generation and propagation analysis via simple monte carlo simulations," presented at the 2010 AAS/AIAA Space Flight Mechanics Conference, San Diego, CA, 2010, Paper No. AAS 10-134.

[13] K. T. Alfriend and J. I. Lim, "Performance of a dynamic algorithm for processing uncorrelated tracks," Proceedings of the AAS/AIAA Astrodynamics Specialist Conference, Girdwood, AK, 1999, Paper No. AAS 99-365.

[14] R. H. Battin, *An Introduction to the Mathematics and Methods of Astrodynamics*, New York: AIAA, 1987.

[15] J. Junkins *et al*., "Non-Gaussian error propagation in orbit mechanics," *Journal of the Astronautical Sciences*, vol. 44, no. 4, October–December 1996, pp. 541–563.

[16] B. D. Tapley *et al*., *Statistical Orbit Determination*. Burlington, MA: Elsevier Academic Press, 2004.

[17] D. Vallado and W. McClain, *Fundamentals of Astrodynamics and Applications* (3rd ed.). El Segundo, CA: Microcosm Press, 2007.

INITIAL DISTRIBUTION LIST

1. Defense Technical Information Center
   Ft. Belvoir, Virginia

2. Dudley Knox Library
   Naval Postgraduate School
   Monterey, California